

## Petrogenesis of lunar mare basalt meteorite Miller Range 05035

Yang LIU<sup>1\*</sup>, Christine FLOSS<sup>2</sup>, James M. D. DAY<sup>3</sup>, Eddy HILL<sup>1,4</sup>, and Lawrence A. TAYLOR<sup>1</sup>

<sup>1</sup>Planetary Geosciences Institute, Department of Earth & Planetary Sciences, University of Tennessee, Knoxville, Tennessee 37996, USA

<sup>2</sup>Laboratory for Space Sciences and Physics Department, Washington University, Saint Louis, Missouri 63130, USA

<sup>3</sup>Department of Geology, University of Maryland, College Park, Maryland 20742, USA

<sup>4</sup>Lunar and Planetary Laboratory, The University of Arizona, Tucson, Arizona 85721, USA

\*Corresponding author. E-mail: yangl@utk.edu

(Received 24 March 2008; revision accepted 31 October 2008)

**Abstract**—Miller Range (MIL) 05035 is a low-Ti mare basalt that consists predominantly of pyroxene (62.3 vol%) and plagioclase (26.4 vol%). Pyroxenes are strongly shocked and complexly zoned from augite (Wo<sub>33</sub>) and pigeonite (Wo<sub>17</sub>) cores with Mg# = 50–54 to hedenbergite rims. Coexisting pyroxene core compositions reflect crystallization temperatures of 1000 to 1100 °C. Plagioclase has been completely converted to maskelynite with signs of recrystallization. Maskelynite is relatively uniform in composition (An<sub>94</sub>Ab<sub>6</sub>–An<sub>91</sub>Ab<sub>9</sub>), except at contacts with late-stage mesostasis areas (elevated K contents, An<sub>82</sub>Ab<sub>15</sub>Or<sub>3</sub>). Symplectites (intergrowth of Fe-augite, fayalite, and silica) of different textures and bulk compositions in MIL 05035 suggest formation by decomposition of ferro-pyroxene during shock-induced heating, which is supported by the total maskelynitization of plagioclase, melt pockets, and the presence of a relict pyroxferroite grain. Petrography and mineral chemistry imply that crystallization of MIL 05035 occurred in the sequence of Fe-poor pyroxenes (Mg# = 50–54), followed by plagioclase and Fe-rich pyroxenes (Mg# = 20–50), and finally hedenbergite, Fe-Ti oxides, and minor late-stage phases. Petrography, bulk chemistry, mineral compositions, and the age of MIL 05035 suggest it is possibly source crater-paired with Asuka (A-) 881757 and Yamato (Y-) 793169, and may also be launch-paired with Meteorite Hills (MET) 01210. MIL 05035 represents an old (~3.8–3.9 Ga), incompatible element-depleted low-Ti basalt that was not sampled during the Apollo or Luna missions. The light-REE depleted nature and lack of Eu anomalies for this meteorite are consistent with an origin distant from the Procellarum KREEP Terrane, and genesis from an early cumulate mantle-source region generated by extensive differentiation of the Moon.

### INTRODUCTION

Lunar meteorites greatly extend our ability to understand magmatic processes on the Moon (e.g., Korotev 2005; Day et al. 2007). Among over 130 lunar meteorites found on the Earth to date, there are approximately 10 unbrecciated mare basalts, including Asuka (A-) 881757, Dhofar 287, LaPaz Icefield (LAP) 02205, 02224, 02226, 02436, 03632, and 04841, Northeast Africa (NEA) 003, Northwest Africa (NWA) 032/479, 773, 4734, 4898, and Yamato (Y-) 793169. Although a number of these samples are paired, they provide invaluable insights into the timing, compositional variation, and mantle sources of mare basalts. For example, A-881757 and Y-793169 have similar bulk compositions, cosmic-ray exposure, and crystallization ages, and are likely source crater-paired (Warren and Kallemeyn 1993; Thalmann et al. 1996; Korotev et al. 2003; Fernandes et al. 2005). NWA 032 and the LAP meteorites are considered to be paired and likely derive from

the Procellarum KREEP (potassium, rare-earth element, phosphor-rich) Terrane (e.g., Day et al. 2006a; Day and Taylor 2007), and Dhofar 287 mainly consists of a crystalline mare basalt that is distinctly different from the other mare basalt meteorites, given its KREEPy nature (Anand et al. 2003a).

Miller Range (MIL) 05035 (~142 g) was found in the Miller Range Icefield, Antarctica, during the 2005 Antarctic Search for Meteorites Program field season (Antarctic Meteorite Newsletter 2006). It is a coarsely crystalline (crystal grains up to 5 mm in length), unbrecciated mare basalt consisting primarily of pyroxene and plagioclase grains. Oxygen isotope values for MIL 05035 are consistent with a lunar origin (Joy et al. 2008). In this contribution, we report the petrography and mineral and bulk rock chemistry of this meteorite. We have studied two polished sections (.6 and .40) with a total area of ~2.1 cm<sup>2</sup>, and a 1.9 g rock chip (MIL 05035, 20), which is being used for ongoing geochemical investigation of this meteorite. These data, combined with

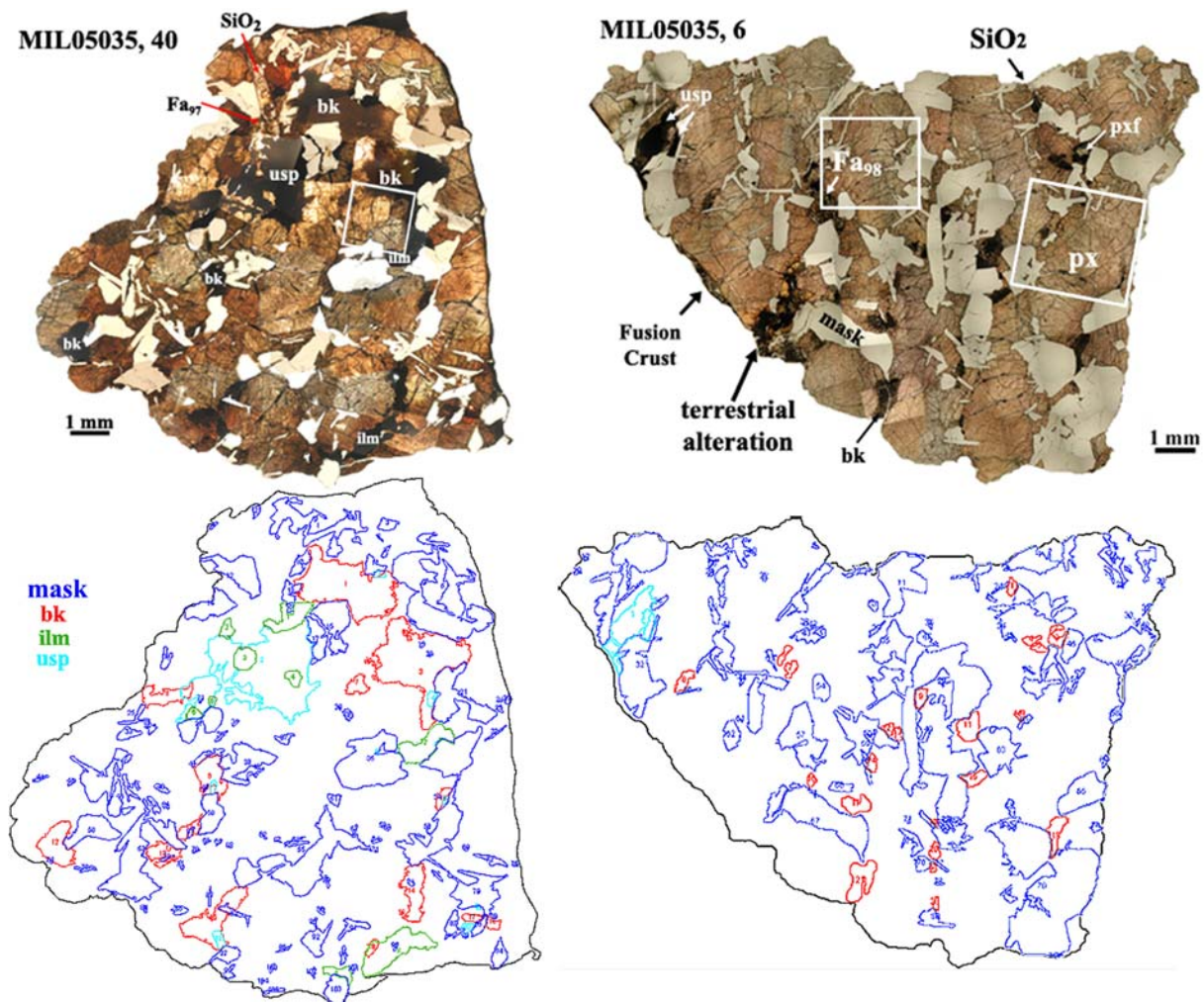


Fig. 1. Photo-mosaics of MIL 05035,6 and 40 in transmitted light and examples of ImageJ results for each section. The variation of color in photomosaics is the result of different degrees of exposure for the individual images. Abbreviations are bk for symplectites, ilm for ilmenite, mask for maskelynite, px for pyroxene, pxf for pyroxferroite, SiO<sub>2</sub> for the silica phase (tridymite), and usp for ulvöspinel. In ImageJ, the colored photo was first converted to a high-resolution grayscale bitmap. A given phase was detected and measured after setting a threshold according to its gray color. Each measured grain of the same phase was outlined by showing its measured perimeter. Black curves outline the total area measured, blue curves outline maskelynite, red curves outline symplectites, cyan color indicates ulvöspinel, and green curves are ilmenite. For clarity, other phases and cracks are not labeled. Boxes outline pyroxenes imaged in Fig. 3.

several preliminary reports and the most recent work of Joy et al. (2008), permit detailed analysis of the petrogenesis of MIL 05035. We demonstrate that MIL 05035 is likely source-paired with A-881757 and Y-793169, but not necessarily with MET 01210, and is derived from an ancient incompatible element-depleted lunar mantle source.

## ANALYTICAL METHODS

### Modal Analysis

Polished thin-sections of MIL 05035 were carefully examined with a petrographic microscope in order to characterize their mineralogical and textural variations. Image analysis software (Freeware ImageJ, NIH) was employed to analyze mineral modes within the photo-mosaics

(Fig. 1 and Table 1). To do this, photo-mosaics of each section were taken in plane-polarized, transmitted-light and converted to high-resolution grayscale images where plagioclase (bright in transmitted light, thus higher grayscale number) and opaque phases (dark, lower grayscale number) were readily distinguishable (Fig. 1). Individual opaque phases (ulvöspinel, ilmenite, and symplectite) were classified with the aid of an optical microscope and then manually defined on the photo-mosaics. Using ImageJ, a single phase was selected by setting a threshold with a minimum and a maximum grayscale number. The areas (total number of pixels) of individual grains were measured directly. Abundances of pyroxene were determined by the difference between total area and the sum of other phases. Uncertainties for this method were caused by choices of the threshold values and have been previously described in Day et al.

Table 1. Modal abundances (in vol%) for lunar meteorite MIL 05035 compared with other mare basalts.

Section #	Crystalline, mare basalt meteorites								Apollo mare basalts				
	MIL 05035							A-881757	Y-793169	12016	12054	15556	
	6	40	29 <sup>a</sup>	33 <sup>a</sup>	36 <sup>a</sup>	31 <sup>b</sup>	34 <sup>b</sup>	Avg. <sup>c</sup>			25	136	
Area (cm <sup>2</sup> )	1.08	1.03	1.00	0.92	0.81	0.6	1.44						
<i>Data source</i>	1	1	2	2	2	3	3		4	5	6	6	7
Pyroxene	66.9	63.7	58.7	69.2	63.4	54.0	61.4	62.3	59	56	52.1	62.1	57
Feldspar/maskelynite	29.0	20.2	35.0	17.2	29.5	36.3	24.8	26.4	30	42	29.1	27.9	38
Olivine/fayalite	1.9	0.0	n.a.	n.a.	n.a.	0.60	3.51	1.8	n.a.	n.a.		0.1	
Silica	0.3	0.8	n.a.	n.a.	n.a.	0.83	1.13	0.8	n.a.	n.a.		1	0.8
Ulvöspinel	0.5	4.3	n.a.	n.a.	n.a.	0.16	0.84	1.5	<5	1		0.5	4.4
Ilmenite	0.0	2.6	n.a.	n.a.	n.a.	0.54	0.82	1.0	6	1	4.8	5.2	2.1
Troilite	0.2	n.a.	n.a.	n.a.	n.a.	0.21	0.16	0.1	<5			0.3	0.1
Symplectites <sup>d</sup>	1.2	8.4	n.a.	n.a.	n.a.	6.24	6.77	5.7	<5				
Phosphate	n.a.	n.a.	n.a.	n.a.	n.a.	0.65	0.06	0.2					
Opaque phases	–	–	6.3	13.6	7.0	–	–	–	<5	2	4.8	8	3.2
Mesostasis	n.a.					3.55	7.06				0.6	1.9	1

Data sources: 1. This study; 2. Arai et al. (2007); 3. Joy et al. (2008); 4. Yanai and Kojima (1991); 5. Takeda et al. (1993); 6. Neal et al. (1994); 7. Rhodes and Hubbard (1973). n.a. = not analyzed.

<sup>a</sup>Opaque phases reported in Arai et al. (2007) include oxides, troilite, mesostasis, and symplectite.

<sup>b</sup>Mesostasis in MIL 05035 by Joy et al. (2008) includes silica, fayalite, troilite, phosphate, and glass.

<sup>c</sup>Average modal abundances were calculated using data for sections 6, 40, 31, and 34 of MIL 05035, corrected proportionally to their surface area.

<sup>d</sup>Symplectites refer to intergrowth of pyroxene, fayalite, and SiO<sub>2</sub>.

Table 2. Modal abundance of minerals in symplectites and their reconstructed bulk compositions.

	bk1	bk2	bk3	Myrmekitic bk8	Myrmekitic bk5
Volume percentage of minerals in symplectite <sup>a</sup>					
Olivine (Fa <sub>94</sub> )	46.6 (1.3)	44.8 (0.3)	51.0	43.9	24.2
Silica	21.3 (1.7)	21.1 (0.9)	16.5	22.2	8.3
Pyroxene (En <sub>10</sub> Fs <sub>55</sub> )	32.1 (2.8)	34.0 (1.1)	32.5	34.0	67.4
N <sub>area</sub> <sup>b</sup>	3	3	2	1	2
Reconstructed bulk compositions					
SiO <sub>2</sub>	46.6	46.5	43.8	47.9	48.5
TiO <sub>2</sub>	0.34	0.39	0.35	0.25	0.68
Al <sub>2</sub> O <sub>3</sub>	0.29	0.27	0.25	0.17	0.76
Cr <sub>2</sub> O <sub>3</sub>	0.03	0.03	0.02	0.02	0.07
MgO	2.92	2.13	2.33	2.32	3.52
CaO	5.20	5.79	5.69	5.19	9.95
MnO	0.68	0.63	0.65	0.56	0.55
FeO	43.6	44.0	46.6	43.3	35.8
Na <sub>2</sub> O	0.01	0.02	0.02	0.01	0.02
En	9.4	6.9	7.2	7.6	11.5
Fs	78.6	79.7	80.3	80.1	65.3
Wo	12.0	13.4	12.6	12.3	23.2

<sup>a</sup>Numbers in parentheses represent variations among the three measured areas. Mineral compositions are reported in Table 3.

<sup>b</sup>N<sub>area</sub> is the number of different areas analyzed in the symplectite.

(2006b). Varying threshold settings results in about 1% relative error for major phases and ~10% relative error for minor phases.

Back-scattered electron (BSE) images of several regions within individual symplectites were collected using a CAMECA SX50 electron microscope at the University of Tennessee. The mineral modes of the symplectites were measured on these BSE images using the protocol for modal analysis outlined above. Olivine (white), pyroxene (light gray), and tridymite (dark gray) were readily distinguished by their varied gray hues. Cracks (dark regions in BSE images) in the sample were excluded from measurement. Bulk compositions of symplectites were reconstructed using the modal percentage of minerals, the measured compositions of the minerals (see below), and their corresponding densities (Table 2).

### Mineral Chemistry

Major- and minor-element compositions of minerals were determined using CAMECA SX-50 and SX-100 electron microprobes (EMP) housed at the University of Tennessee (Tables 3 and 4). The analytical conditions for pyroxenes and oxides employed an accelerating potential of 15 kV, a 20 nA beam current, a 1 μm beam size, and standard PAP correction procedures. For maskelynite, troilite, apatite, and fusion-crust glass, a lower beam current (10 nA) and a defocused beam size (5 μm) were used to minimize thermal deterioration of the minerals and migration of volatile elements (e.g., Na, K). The counting time for all elements was 20 s except for La and Ce in apatite (40 s) and Zr in Fe-Ti oxides (50 s). The detection limits (3σ above background) were 0.03 wt% for SiO<sub>2</sub>, TiO<sub>2</sub>, Al<sub>2</sub>O<sub>3</sub>,

MgO, CaO, Na<sub>2</sub>O and K<sub>2</sub>O; 0.05 wt% for Cr<sub>2</sub>O<sub>3</sub>, MnO, FeO, P<sub>2</sub>O<sub>5</sub>; and 0.05–0.1 wt% for all other oxides and elements listed. In order to obtain a more precise analysis of ZrO<sub>2</sub> in Fe-Ti oxides, a 200 s counting time was used for Zr and the detection limit (3σ) for ZrO<sub>2</sub> is 0.02 wt%.

Trace-element compositions of pyroxenes and maskelynites (Tables 5 and 6) were analyzed on a modified CAMECA IMS-3f ion microprobe at Washington University, following the procedure outlined in Zinner and Crozaz (1986a). Secondary ions were generated using an O<sup>-</sup> primary beam with an accelerating voltage of 12.5 kV. The elemental concentrations were measured by counting secondary ions of individual isotopes and comparing to the counts of a reference element, Si in this case. The concentrations of SiO<sub>2</sub> for the specific grain were determined using the CAMECA SX-50 at the University of Tennessee. Energy filtering (100 V offset) were used at low mass-resolution to remove complex molecular interferences. The resulting spectrum was deconvolved to remove interferences from simple molecules for elements K-Ca-Sc-Ti, Rb-Sr-Y-Zr, and Ba-REE (Alexander 1994). Sensitivity factors for rare-earth elements (REEs) for pyroxenes and plagioclases are from Zinner and Crozaz (1986b), and those for other elements are from Hsu (1995), as listed in Table 1 of Floss et al. (1998). Errors (1σ) for ion probe analyses were estimated from the counting statistics.

### Bulk Rock Chemistry

A 1.9 g subsample (20) of MIL 05035 was disaggregated and homogenized to a powder in a high-purity alumina mortar and pestle, under clean laboratory conditions. The mortar and pestle employed are used exclusively for mare basalts, and were

Table 3. Representative silicate mineral major-element compositions in MIL 05035.

Association <sup>a</sup>	Pyroxenes				Pyroxferroite	Maskelynite		Olivine			Feldspar	
	Prm-core <sup>b</sup>	Prm-core <sup>b</sup>	Prm-rim	Bk <sup>c</sup>		core	rim	Prm	rim of usp	Bk <sup>c</sup>	in FeS	in Fayalite
SiO <sub>2</sub>	49.9	49.9	46.9	47.7(3)	46.4(2)	45.4	47.7	29.4	30.2	33.2(3)	55.9	55.9
TiO <sub>2</sub>	0.63	0.97	0.96	0.91(6)	0.37(3)	–	–	0.11	0.32	0.15(15)	–	–
Al <sub>2</sub> O <sub>3</sub>	1.11	1.84	0.88	0.82(8)	0.24(1)	34.1	31.9	<0.03	<0.03	<0.03	20.3	20.3
Cr <sub>2</sub> O <sub>3</sub>	0.46	0.62	<0.05	0.06(2)	<0.05	–	–	<0.05	0.14	<0.05	–	–
MgO	14.2	12.1	1.36	2.60(3)	2.51(13)	0.12	<0.03	0.69	3.78	3.08(21)	–	–
CaO	6.86	15.9	15.0	17.1(1)	5.96(15)	18.5	16.8	0.58	0.39	0.45(5)	0.16	0.16
MnO	0.50	0.31	0.41	0.49(4)	0.69(7)	–	–	0.69	0.71	0.79(3)	–	–
FeO	25.9	18.6	34.2	30.4(6)	43.5(3)	0.48	0.84	68.5	64.9	62.0(7)	0.98	1.17
Na <sub>2</sub> O	<0.03	<0.03	<0.03	0.05(2)	<0.03	0.75	1.56	–	–	–	0.26	0.43
K <sub>2</sub> O	–	–	–	–	–	0.03	0.23	–	–	–	11.6	12.3
BaO	–	–	–	–	–	–	–	–	–	–	10.9	7.99
Total	99.6	100.3	99.7	100.1	99.7	99.4	99.0	100.0	100.5	99.7	100.0	100.0
O	6	6	6	6	6	8	8	4	4	4	8	8
Si	1.947	1.916	1.956	1.958	1.976	2.109	2.216	0.993	0.991	1.007	2.783	2.823
Ti	0.019	0.028	0.030	0.030	0.011			0.003	0.008	0.001		
Al	0.051	0.083	0.043	0.042	0.011	1.867	1.747				1.190	1.147
Cr	0.014	0.019										
Mg	0.823	0.693	0.085	0.158	0.159	0.008		0.035	0.185	0.121		
Ca	0.286	0.656	0.670	0.750	0.272	0.921	0.836	0.021	0.014	0.016	0.010	0.029
Mn	0.016	0.010	0.014	0.018	0.025			0.020	0.020	0.029		
Fe	0.844	0.599	1.192	1.040	1.550	0.019	0.033	1.933	1.780	1.813	0.040	0.048
Na	0.001	0.002	0.001			0.068	0.141				0.027	0.041
K						0.002	0.014				0.733	0.767
Ba											0.213	0.153
Total	4.00	4.01	3.99	4.00	4.01	4.99	4.99	3.00	3.00	2.99	5.00	5.01
Mg#	49.4	53.6	6.7	13.2	9.3			1.8	9.4	6.3		

<sup>a</sup>Abbreviations indicate the type of mineral and its association. "Prm" represents primary; "Bk" indicates symplectite. Feldspars are associated with troilite (FeS) or fayalite.

<sup>b</sup>Compositions of two pyroxenes appear in the core.

<sup>c</sup>Pyroxferroite and minerals in symplectites are relatively uniform. Numbers in parentheses for these minerals represent 1 $\sigma$  (based on multiple analyses) of least units cited.

Table 4. Representative compositions of oxides, apatite, and glass in MIL 05035.

Assoc. <sup>c</sup>	Glass in Fa		Ulvöspinel <sup>a</sup>		Ilmenite <sup>a</sup>			Apatite <sup>b</sup>	Fusion crust <sup>d</sup>
	K-Si	K-Ca	Prm	Mes	Prm	Mes-Sp	Fa		
SiO <sub>2</sub>	78.0	79.5	0.05	0.09	0.03	0.06	<0.03	0.61	46.5(8)
TiO <sub>2</sub>	–	–	30.2	21.1	52.5	52.9	52.5	–	0.66(6)
Al <sub>2</sub> O <sub>3</sub>	11.1	11.7	2.11	2.85	0.06	<0.03	0.04	–	18.1(101)
Cr <sub>2</sub> O <sub>3</sub>	–	–	5.34	22.6	0.11	0.22	<0.05	–	0.12(10)
MgO	–	–	0.18	0.15	0.28	0.18	0.06	0.01	2.76(216)
CaO	0.12	4.48	<0.03	0.20	<0.03	0.08	0.03	53.8	14.0(20)
MnO	–	–	0.32	0.31	0.37	0.35	0.38	–	0.22(14)
FeO	0.61	0.37	61.4	52.0	45.6	46.6	46.4	2.14	13.8(97)
Na <sub>2</sub> O	0.13	0.37	–	–	–	–	–	0.03	0.75(47)
K <sub>2</sub> O	10.3	3.29	–	–	–	–	–	–	0.11(8)
BaO	0.11	<0.05	–	–	–	–	–	–	–
P <sub>2</sub> O <sub>5</sub>	–	–	–	–	–	–	–	40.6	0.22(6)
La <sub>2</sub> O <sub>3</sub>	–	–	–	–	–	–	–	0.17	–
Ce <sub>2</sub> O <sub>3</sub>	–	–	–	–	–	–	–	0.26	–
ZrO <sub>2</sub>	–	–	<0.02	0.04	n.a.	0.28	0.26	–	–
V <sub>2</sub> O <sub>3</sub>	–	–	–	0.56	–	<0.05	–	–	–
F	–	–	–	–	–	–	–	1.72	–
Cl	–	–	–	–	–	–	–	0.52	–
Total	100.4	99.7	99.6	99.9	99.0	100.7	99.7	100.1	99.6
–O = F,Cl								0.84	–
O	24	24	4	4	3	3	3	24	–
Si	10.23	10.19	0.002	0.003	–	0.002	–	0.099	–
Ti	–	–	0.845	0.584	1.003	0.997	1.001	–	–
Al	1.720	1.771	0.093	0.124	0.002	0.000	0.001	–	–
Cr	–	–	0.157	0.657	0.002	0.004	0.001	–	–
Mg	–	–	0.010	0.008	0.011	0.007	0.002	0.008	–
Ca	0.020	0.615	–	0.008	–	0.000	–	9.422	–
Mn	–	–	0.010	0.010	0.008	0.005	0.008	–	–
Fe	0.070	0.040	1.912	1.603	0.967	0.975	0.984	0.292	–
Na	0.030	0.092	–	–	–	–	–	0.009	–
K	1.710	0.538	–	–	–	–	–	–	–
Ba	0.010	0.003	–	–	–	–	–	–	–
P	–	–	–	–	–	–	–	5.614	–
La	–	–	–	–	–	–	–	0.010	–
Ce	–	–	–	–	–	–	–	0.015	–
Zr	–	–	–	0.001	–	0.002	0.004	–	–
V	–	–	–	0.017	–	0.000	–	–	–
Total	13.8	13.2	3.03	3.01	1.99	1.99	2.00	15.5	–

<sup>a</sup>Counting time for Zr was 200 s, which yields a detection limit (3 $\sigma$ ) of 0.02 wt% ZrO<sub>2</sub>.

<sup>b</sup>Total cations of apatite shows deficiency from stoichiometric value (16), suggesting significant rare elements as reported in Joy et al. (2008).

<sup>c</sup>Compositions of mineral phases are presented according to their association with other phases. “Prm” represents primary; “Mes” indicates mesostasis; “Sp” represents spinel; and “Fa” represents fayalite. Glass in fayalite was found to be K-Si rich or K-Ca rich.

<sup>d</sup>Numbers in parentheses represent 1 $\sigma$  of least units cited, obtained from multiple analyses on fusion crust. For example 1.81(101) stands for 1.81  $\pm$  1.01.

thoroughly abraded with high-purity quartz powder and washed in dilute HCl and 18.3 M $\Omega$  water prior to use. Approximately 20 mg from the 1.9 g aliquot of well-homogenized, whole-rock powder was melted on a Mo-strip heater, in a nitrogen atmosphere, to generate a fused bead. Major-element concentrations in the fused bead were analyzed using the Cameca SX-50 electron microprobe, with a defocused beam of 15 kV voltage, 10 nA current, and a 5  $\mu$ m diameter. Concentrations of minor and trace elements in the fused bead were determined using a New Wave Research UP213 (213 nm) laser-ablation system, coupled to a

ThermoFinnigan Element 2 ICP-MS at the University of Maryland. Ablation analysis took place in a 3 cm<sup>3</sup> cell with a He atmosphere. The cell was flushed with a He gas flow of 1 L/min to enhance production of fine aerosols, and the gas was mixed with an Ar carrier gas flow of 0.4 L/min before reaching the torch. The fused bead was analyzed with a 150 m beam size, long raster paths to ensure homogenization, and a laser repetition rate of 7 Hz at 2 to 2.5 J/cm<sup>2</sup>. Th/ThO production was ~0.07% for all analytical sessions. Each analysis consisted of ~60 s of data collection and 20 s of background on the ICP-MS sample gas. Washout time between spots was greater than 2

Table 5. Major and trace-element concentrations of maskelynite in MIL05035,6.

wt%	M16 rim	M16 center <sup>a</sup>	M13 rim	M13 pt2 center	M15 center	M14 rim						
SiO <sub>2</sub>	45.6	45.2	46.8	45.2	45.1	47.1						
Al <sub>2</sub> O <sub>3</sub>	33.4	33.8	32.7	33.7	33.7	32.0						
MgO	<0.03	0.06	<0.03	0.07	0.10	0.05						
CaO	17.7	18.6	17.3	18.4	18.3	17.1						
FeO	0.57	0.50	0.92	0.65	0.51	0.65						
Na <sub>2</sub> O	1.15	0.85	1.35	0.94	0.79	1.44						
K <sub>2</sub> O	0.08	<0.03	0.19	0.05	<0.03	0.20						
Total	98.5	99.0	99.3	99.0	98.5	98.5						
An	89.1	92.3	86.6	91.3	92.7	85.8						
Ab	10.5	7.61	12.2	8.41	7.27	13.0						
Or	0.5	0.1	1.2	0.3	0	1.2						
p.p.m.		±1σ	±1σ	±1σ	±1σ	±1σ	±1σ					
Sc	3.1	0.1	3.4	0.2	3.4	0.1	2.9	0.1	3.0	0.1	2.8	0.1
Ti	73.5	0.6	112.4	0.8	90.2	0.6	120.8	0.5	118.8	0.8	97.8	0.6
V	1.13	0.05	2.06	0.08	1.76	0.06	2.19	0.05	1.70	0.07	1.25	0.05
Cr	0.55	0.05	1.46	0.09	1.40	0.07	2.56	0.07	1.21	0.07	0.59	0.03
Mn	114	1	127	1	120	1	111	0	113	1	107	1
Fe	3768	29	3399	33	3354	26	3078	20	3363	29	3741	26
Sr	373	1	229	1	272	1	233	1	250	1	352	1
Y	0.38	0.02	0.26	0.02	0.25	0.01	0.24	0.01	0.26	0.01	0.32	0.02
Zr	0.03	0.01	0.05	0.01	0.04	0.01	0.03	0.01	0.03	0.01	0.04	0.01
Nb	0.00	0.00	0.00	0.00	0.00	0.00	0.00	0.00	0.00	0.00	0.00	0.00
Ba	27.43	0.43	11.78	0.33	14.74	0.30	12.04	0.21	13.63	0.32	23.89	0.35
La	0.22	0.02	0.18	0.02	0.16	0.01	0.17	0.01	0.19	0.01	0.26	0.02
Ce	0.58	0.03	0.36	0.04	0.36	0.03	0.34	0.02	0.41	0.02	0.59	0.05
Pr	0.08	0.01	0.05	0.01	0.05	0.01	0.06	0.00	0.05	0.01	0.07	0.01
Nd	0.34	0.02	0.21	0.02	0.23	0.01	0.26	0.01	0.25	0.01	0.34	0.01
Sm	0.08	0.01	0.05	0.01	0.06	0.01	0.07	0.01	0.06	0.01	0.10	0.01
Eu	2.87	0.09	1.59	0.08	1.93	0.07	1.64	0.05	1.84	0.06	2.70	0.07
Gd	0.10	0.01	0.05	0.01	0.07	0.01	0.07	0.01	0.06	0.01	0.08	0.01
Tb	0.01	0.00	0.01	0.00	0.01	0.00	0.01	0.00	0.01	0.00	0.02	0.00
Dy	0.07	0.01	0.05	0.01	0.06	0.01	0.05	0.00	0.05	0.01	0.08	0.01
Ho	0.02	0.00	0.01	0.00	0.02	0.00	0.01	0.00	0.02	0.00	0.02	0.00
Er	0.04	0.01	0.03	0.01	0.03	0.01	0.04	0.00	0.03	0.01	0.04	0.01
Tm	u.d.	u.d.	0.00	0.01	0.01	0.01	u.d.		u.d.		0.01	0.01
Yb	0.03	0.01	0.02	0.01	0.03	0.01	0.05	0.01	0.04	0.01	0.03	0.01
Lu	0.00	0.00	0.00	0.00	u.d.		u.d.		0.00	0.00	0.00	0.00
Eu/Eu*	97.1		94.6		90.9		70.0		94.5		92.2	

<sup>a</sup>Analyses were used to calculate parental melt compositions. u.d. = Under limits of analytical detection.

minutes. Raw data were analyzed and corrected using the LAM-Trace software program. Data were collected in time-resolved mode so that effects of inhomogeneities in the bead could be evaluated for each analysis; such effects were found to be negligible. LA-ICP-MS analyses were normalized to CaO measured previously by electron microprobe, as an internal standard to account for variable ablation yield. This internal normalization is supported by a small relative difference (<2%) in EMP Ca content over a 150 μm spot. The NIST 610 glass standard was used for calibration of relative element sensitivities and replicate LA-ICP-MS analyses of the BIR-1g glass standard are presented with the new MIL 05035 bulk rock data in Table 7.

## RESULTS

### Petrography and Mineral Compositions

MIL 05035 is a coarse crystalline, unbrecciated rock, consisting mainly of pyroxene (>2 mm) and maskelynite (>1 mm) grains (Fig. 1 and Table 1). The abundances of pyroxene (63.7–66.9 vol%) and maskelynite (20.2–29.0 vol%), from the two thin-sections examined, are within the ranges determined on five other sections (54.0–69.2 vol% for pyroxene; 17.2–36.3 vol% for plagioclase/maskelynite) by Arai et al. (2007) and Joy et al. (2008). Minor minerals in this meteorite include ulvöspinel, ilmenite, fayalite, silica, troilite,

Table 6. Major- and trace-element concentrations of pyroxenes in MIL05035,6.

wt%	Px2pt1 <sup>a</sup>	Px2pt2	Px2pt3	Px2pt4	Px8pt1 <sup>a</sup>	Px8pt5	Px8pt4	Px1pt4	Px1pt3	Px1pt2 <sup>a</sup>	Px1pt1	Px11pt2	Px14pt2	Px14pt1	Pfx	Px ^BK2	Px ^BK5
SiO <sub>2</sub>	49.6(4)	49.5(4)	49.5(2)	49.8(1)	49.8(3)	48.0(1)	48.9(1)	49.6(0)	48.0(2)	46.3(2)	46.2(5)	46.7(2)	48.8(2)	48.9(2)	46.5(2)	47.4(7)	46.8(2)
TiO <sub>2</sub>	0.96(10)	1.04(3)	0.78(5)	0.70(8)	0.66(5)	0.92(11)	1.07(4)	0.78(5)	0.99(5)	0.93(2)	1.22(3)	0.97(5)	0.88(6)	0.78(5)	0.36(3)	1.13(8)	1.03(8)
Al <sub>2</sub> O <sub>3</sub>	1.78(19)	1.91(5)	1.24(9)	1.26(18)	1.20(13)	1.04(17)	1.57(9)	1.47(11)	1.06(9)	0.87(3)	0.91(5)	0.93(5)	1.17(5)	1.12(3)	0.23(2)	1.10(11)	1.10(6)
Cr <sub>2</sub> O <sub>3</sub>	0.63(7)	0.65(4)	0.45(3)	0.44(10)	0.45(3)	0.23(4)	0.51(4)	0.54(4)	0.20(6)	0.07(3)	0.05(1)	0.09(3)	0.40(4)	0.40(2)	<0.05	0.05(2)	0.06(2)
MgO	12.1(4)	11.4(2)	12.0(2)	13.1(4)	14.0(1)	8.50(37)	9.84(13)	13.3(3)	7.93(86)	3.04(38)	0.86(6)	3.67(57)	10.3(3)	11.2(6)	2.54(11)	3.06(19)	2.86(15)
CaO	14.0(20)	16.4(6)	9.13(141)	7.69(175)	7.03(41)	7.34(73)	14.7(4)	8.86(76)	10.3(8)	10.5(8)	18(6)	11.9(7)	9.57(30)	8.01(42)	6.02(9)	17.7(3)	15.9(3)
MnO	0.37(4)	0.35(4)	0.44(3)	0.47(3)	0.46(4)	0.55(6)	0.39(1)	0.43(2)	0.49(3)	0.52(3)	0.30(2)	0.51(3)	0.48(5)	0.51(2)	0.63(2)	0.41(3)	0.41(3)
FeO	19.9(17)	17.7(3)	26.1(13)	25.7(18)	25.8(4)	32.9(9)	22.1(5)	24.2(6)	30.2(21)	37.1(5)	31.2(2)	34.4(12)	27.7(4)	28.4(9)	43.4(2)	28.2(10)	31.1(7)
Na <sub>2</sub> O	0.04(2)	0.05(1)	0.03(1)	0.04(1)	<0.03	<0.03	0.04(2)	0.03(1)	0.03(0)	0.03(2)	0.05(2)	0.04(2)	0.04(2)	0.04(1)	<0.03	0.05(2)	0.03(1)
Total	99.4	99.0	99.6	99.1	99.4	99.5	99.2	99.2	99.2	99.3	98.8	99.2	99.4	99.3	99.7	99.1	99.2
En	36	35	36	40	42	26	30	40	25	10	3	12	32	34	8	10	9
Fs	34	30	44	44	43	57	38	41	53	66	56	61	48	48	78	50	55
Wo	30	36	20	17	15	16	32	19	23	24	41	27	21	18	14	40	36
ppm																	
Sc	145(1)	169(2)	101(1)	80.6(7)	93.6(9)	119(1)	160(1)	119(1)	132(1)	150(1)	85.7(7)	167(1)	122(1)	120(1)	87.8(4)	153(1)	117(1)
Ti	5061(10)	5534(13)	4082(10)	2916(6)	3180(7)	4890(9)	5656(12)	4176(10)	5262(9)	4689(9)	6550(11)	5034(8)	4576(11)	3747(8)	1795(3)	6416(11)	4705(9)
V	174(1)	195(1)	90.6(10)	84.4(6)	99.3(9)	54.1(7)	128(1)	143(1)	70.0(6)	19.0(4)	12.0(4)	26.4(4)	91.2(11)	58.3(8)	4.08(13)	27.8(5)	14.6(4)
Cr	4827(9)	5334(11)	3094(8)	2966(5)	3383(7)	1516(5)	3803(9)	4297(10)	1890(4)	497(3)	292(2)	698(3)	3052(9)	1641(5)	57.3(6)	537(3)	363(3)
Mn	3604(7)	3119(8)	4920(10)	5018(7)	4574(9)	5498(10)	3921(9)	4481(10)	5024(8)	6005(11)	3240(8)	5347(9)	4852(12)	4703(10)	6986(8)	4591(10)	5027(11)
Rb	u.d.	1.30(54)	0.95(40)	0.23(18)	0.24(19)	0.11(37)	0.48(56)	0.91(37)	0.39(37)	0.67(49)	u.d.	0.36(53)	1.01(41)	0.46(46)	0.05(31)	0.71(94)	1.71(90)
Sr	7.19(25)	8.70(33)	3.07(19)	1.61(8)	1.67(11)	4.06(20)	7.96(33)	3.30(21)	4.56(19)	6.16(27)	89.8(11)	8.80(26)	3.80(25)	5.49(22)	3.38(14)	35.6(6)	17.8(5)
Y	12.5(3)	15.2(4)	9.19(31)	5.48(16)	5.77(22)	11.8(3)	12.3(4)	9.08(31)	11.5(3)	21.9(4)	108(1)	22.6(4)	9.63(36)	50.0(7)	130(1)	78.9(9)	61.3(8)
Zr	7.03(30)	9.74(35)	6.75(34)	2.26(9)	2.67(14)	9.63(39)	7.80(30)	4.78(23)	5.81(23)	11.7(5)	175(2)	14.3(4)	4.46(24)	11.6(4)	20.9(4)	88.4(15)	62.7(13)
Nb	0.14(2)	0.14(1)	0.44(5)	0.04(0)	0.06(1)	0.08(1)	0.13(2)	0.10(1)	0.06(1)	0.07(1)	0.25(2)	0.05(1)	0.06(1)	0.06(1)	0.05(1)	0.20(3)	0.09(1)
Ba	0.38(5)	0.33(6)	1.70(18)	0.37(4)	0.19(4)	0.29(5)	0.46(6)	0.47(7)	0.44(5)	0.73(7)	2.13(18)	0.67(7)	0.50(7)	1.02(10)	0.45(4)	2.44(27)	0.91(11)
La	0.22(2)	0.24(3)	0.24(3)	0.05(1)	0.09(2)	0.18(3)	0.17(2)	0.15(2)	0.08(1)	0.25(3)	4.15(23)	0.34(4)	0.12(2)	1.28(9)	0.30(3)	3.07(17)	2.62(17)
Ce	0.65(6)	0.85(7)	0.54(6)	0.13(2)	0.22(3)	0.65(6)	0.86(7)	0.33(3)	0.44(4)	1.13(9)	18.5(7)	1.67(12)	0.31(4)	3.33(20)	1.69(9)	11.0(5)	8.02(46)
Pr	0.18(1)	0.21(2)	0.13(2)	0.04(1)	0.06(1)	0.14(2)	0.20(2)	0.08(1)	0.12(1)	0.29(3)	4.27(23)	0.38(3)	0.06(1)	0.76(6)	0.48(3)	1.92(11)	1.76(15)
Nd	1.15(6)	1.32(7)	0.81(6)	0.24(2)	0.36(3)	0.80(5)	1.23(7)	0.63(4)	0.82(4)	1.82(9)	25.8(8)	2.20(11)	0.60(4)	3.91(17)	4.01(16)	11.1(4)	9.2(41)
Sm	0.67(7)	0.89(7)	0.40(4)	0.17(2)	0.25(3)	0.51(4)	0.77(6)	0.36(4)	0.51(5)	1.1(8)	10.7(6)	1.39(11)	0.38(5)	1.79(13)	2.89(16)	5.17(28)	4.43(30)
Eu	0.08(1)	0.09(1)	0.05(1)	0.02(0)	0.03(1)	0.06(1)	0.07(1)	0.03(1)	0.06(1)	0.11(1)	1.24(9)	0.15(1)	0.04(1)	0.11(2)	0.25(2)	0.59(4)	0.39(3)
Gd	1.22(14)	1.48(16)	0.84(11)	0.39(4)	0.41(7)	0.99(11)	1.19(12)	0.69(9)	0.93(11)	1.89(20)	16.3(11)	2.21(20)	0.80(11)	3.22(31)	6.38(47)	8.04(54)	6.30(60)
Tb	0.25(3)	0.34(4)	0.21(3)	0.10(1)	0.11(1)	0.22(3)	0.31(3)	0.15(2)	0.19(2)	0.39(4)	2.91(22)	0.50(5)	0.20(2)	1.04(8)	1.78(12)	1.67(13)	1.52(13)
Dy	1.94(10)	2.38(12)	1.49(9)	0.79(4)	0.96(5)	1.76(10)	2.09(11)	1.52(8)	1.94(10)	3.53(17)	20.9(7)	3.89(18)	1.58(9)	8.59(33)	16.7(5)	12.9(5)	10.1(4)
Ho	0.48(3)	0.52(4)	0.33(4)	0.21(2)	0.24(2)	0.46(4)	0.49(4)	0.28(3)	0.44(4)	0.88(7)	4.74(29)	0.77(6)	0.38(4)	1.81(12)	4.6(20)	2.57(17)	2.13(16)
Er	1.37(8)	1.60(11)	1.23(8)	0.69(4)	0.80(4)	1.43(8)	1.42(8)	0.99(7)	1.46(7)	2.80(14)	11.3(5)	2.81(13)	1.06(7)	5.84(23)	14.9(4)	9.24(34)	6.42(32)
Tm	0.21(2)	0.25(2)	0.15(2)	0.10(1)	0.13(1)	0.21(2)	0.23(2)	0.16(1)	0.22(2)	0.40(4)	1.69(12)	0.42(4)	0.19(2)	0.77(7)	2.60(15)	1.50(10)	1.01(8)
Yb	1.67(13)	1.58(17)	1.36(10)	0.87(5)	1.06(7)	1.70(11)	1.72(14)	1.25(11)	1.76(11)	3.73(21)	12.1(7)	2.90(22)	1.46(12)	5.58(29)	18.0(8)	9.24(46)	6.24(47)
Lu	0.25(3)	0.23(5)	0.26(4)	0.19(2)	0.14(2)	0.31(4)	0.34(4)	0.24(3)	0.33(4)	0.70(8)	2.21(23)	0.61(7)	0.38(5)	0.67(9)	2.86(27)	1.44(12)	1.03(13)
Eu/Eu*	0.28	0.23	0.27	0.23	0.30	0.25	0.23	0.21	0.28	0.23	0.29	0.25	0.24	0.14	0.17	0.28	0.22

<sup>a</sup>Analyses were used to calculate parental melt compositions. u.d. = Under limits of analytical detection.

Table 7. Bulk rock chemistry of MIL 05035, A-881757, Y-793169, and MET 01210.

Source <sup>b</sup> mass mg/g <sup>d</sup>	BCR-2g <sup>a</sup>	MIL 05035			A-881757				Y-793169	MET 01210	
		This study <sup>c</sup>	1	2	3	3	4	4	3	1	5
		20/1.9	140/0.31	3.55	20/13	20/13	108/?	126/?	20/0.5	150	5
SiO <sub>2</sub>		47.0(18)	48.4(3)	45.4	47.1	47.1			46.0	44.0(3)	46.9
TiO <sub>2</sub>		1.44(57)	0.90(1)	1.67	2.45	2.45			2.19	1.55(1)	1.76
Al <sub>2</sub> O <sub>3</sub>		9.26(29)	8.85(7)	11.5	9.96	10.0			11.1	16.6(1)	12.7
Cr <sub>2</sub> O <sub>3</sub>		0.33(7)	0.300(2)	0.17	0.3	0.29	0.28	0.27	0.24	0.270(4)	0.38
MgO		7.44(82)	7.79(6)	6.42	6.2	6.3			5.75	6.20(5)	6.13
CaO		11.8(4)	12.1(1)	12.0	11.5	11.8			11.1	13.0(2)	14.3
MnO		0.32(3)	0.33(3)	0.25	0.34	0.34			0.32	0.22(1)	0.31
FeO		22.0(19)	20.7(2)	21.7	22.0	22.5	23.3	22.6	21.2	16.5(6)	17
Na <sub>2</sub> O		0.26(3)	0.210(2)	0.50	0.25	0.25	0.30	0.28	0.27	0.320(2)	0.35
K <sub>2</sub> O		0.03(3)	0.010(1)	0.40	0.40	0.37	0.37	0.37	0.06	0.060(1)	0.05
P <sub>2</sub> O <sub>5</sub>		0.05(1)	0.020(1)							0.13(1)	0.08
SO <sub>2</sub>		0.11(5)									
Total		100.0	99.6	100	100.4	101.4				98.8	100.0
Mg #		37.8	40.2	34.5	33.5	33.3			32.8	37.7	39.2
Li	9.63(36)	8.45(24)	9.63(5)							8.07(5)	
Sc	32.5(10)	93.7(60)	109(5)		97	96			87	53.4(6)	53
V	436(4)	105(6)	107(6)		88				53	59.8(3)	73
Co	38(8)	23.8(15)	28.1(16)		24.9	24.3	27.9	27.9	21.4	31.8(2)	
Ni	10.9(25)	8.27(344)	11.0(11)		13.5	<35	60	45	7.3(11)	212(4)	
Cu	18.9(4)	5.21(105)	9.64(55)							23.4(1)	
Zn	159(12)	1.81(38)	16.9(1)		1.72	<35	3	3		37.4(1)	
Ga	21.7(6)	3.07(35)	2.96(9)		2.2(8)	2.8	2.5	3	3.0(13)	19.1(4)	
Ge	3.62(51)	1.00(5)	0.12(6)		0.039				2.2(16)		
Rb	45.8(36)	0.57(21)	0.49(1)				2.3	2.8		1.34(15)	
Sr	316(21)	113(11)	105(13)		128	112	110	120	220(20)	163(11)	143
Y	30.7(11)	19.7(6)	22.1(1)							36.8(1)	5.5
Zr	165(8)	32.3(88)	36.4(40)		97	<110	40	50	190(23)	103(14)	3.5
Nb	10.1(9)	1.94(51)	1.15(3)							1.07(7)	
Cs	1.06(12)	0.02(1)	0.030(4)				0.04	0.04		0.09(1)	
Ba	612(61)	28.4(4)	25.8(2)		65	50	30	25	<81	80.8(3)	21
La	24.6(20)	1.87(26)	1.54(8)		3.7	3.3	3.75	3.64	5.3	6.69(21)	14
Ce	49.6(44)	5.28(63)	4.58(28)		10	8.7	11.5	10.3	15.6	13.8(4)	37
Pr	6.09(54)	0.81(8)	0.75(4)							2.12(12)	5
Nd	27.1(20)	4.59(41)	4.24(24)		7.7	7.8	8.9	7.8	10.2(14)	10.7(5)	22
Sm	6.34(48)	1.87(11)	1.77(4)		3.08	2.96	2.96	2.81	4.40	3.58(11)	5
Eu	1.9(20)	0.82(12)	0.72(5)		1.08	1.03	1.07	1.12	1.37	1.11(6)	1.4
Gd	5.96(32)	2.54(8)	2.65(10)				3.86	3.35		4.54(32)	6
Tb	0.96(5)	0.52(2)	0.56(1)		0.83	0.84	0.81	0.72	1.1	0.91(5)	1.1
Dy	5.77(30)	3.66(8)	3.93(21)		5.5	6	5.3	4.5	7.5(11)	5.85(31)	6.5

Table 7. *Continued.* Bulk rock chemistry of MIL 05035, A-881757, Y-793169, and MET 01210.

Source <sup>b</sup> mass mg/g <sup>d</sup>	BCR-2g <sup>a</sup>	MIL 05035			A-881757			Y-793169	MET 01210		
		This study <sup>c</sup>	1	2	3	3	4	4	3	1	5
		20/1.9	140/0.31	3.55	20/13	20/13	108/?	126/?	20/0.5	150	5
Ho	1.2(6)	0.82(3)	0.88(6)		1.24	1.39			1.63(8)	1.26(7)	1.2
Er	3.24(22)	2.33(12)	2.66(7)							3.63(14)	2.9
Tm	0.46(2)	0.36(3)	0.39(2)				0.49	0.36		0.53(3)	0.3
Yb	3.3(18)	2.83(39)	2.78(12)		3.8	3.48	3.64	2.94	4.8	3.54(10)	1.5
Lu	0.46(3)	0.40(6)	0.39(2)		0.56	0.54	0.56	0.49	0.72	0.52(2)	0.1
Hf	4.49(23)	1.21(22)	1.03(4)		2.26	2.18	2.37	2.05	3.08	2.37(10)	
Ta	0.59(4)	0.10(4)	0.060(1)		0.31	0.28	0.23	0.22	0.33(13)	0.10(1)	
W	0.44(2)	0.31(1)	0.010(2)				0.08	0.073		0.69 (21)	
Pb	11.8(11)	0.42(15)	0.39(1)							0.55(2)	
Th			0.28(2)		0.48	0.44	0.43	0.42	0.75(10)	0.86(3)	
U			0.070(4)				0.21	0.11		0.32(2)	

<sup>a</sup>Standard used in LA-ICP-MS analyses.

<sup>b</sup>Data sources: 1. Bulk composition, reported by Joy et al. (2007, 2008); 2. Yanai (1991); 3. Warren and Kallemeyn (1993); 4. Koeberl et al. (1993); 5. Day et al. (2006b) by modal recombination.

<sup>c</sup>A total of 23 spots were analyzed randomly on the fused bead. Numbers in parentheses are 1 $\sigma$  standard deviation of the 23 analyses, cited to the last significant number. For other data, the 1 $\sigma$  uncertainties in parentheses are cited to the last significant number.

<sup>d</sup>Amount of analyzed material versus the homogenized whole-rock powder from which the aliquot was generated.

and apatite. No Fe-metal grains were found in the sections that were studied here, and they have not been found by other groups (Arai et al. 2007; Joy et al. 2007, 2008), which is unusual for Apollo and Luna mare basalts. Both sections contain a highly vesicular and compositionally heterogeneous fusion crust. Because of the coarse-grained nature of the rock, it would appear that the composition of the fusion crust depends on the mineral substrate it is most closely associated with, and which correspondingly contributed to its composition (Day et al. 2006a, their Fig. 12), as detailed by Thaisen and Taylor (Forthcoming). Therefore, the fusion crust shows large variations in compositions (Table 4) and is of little practical use. Terrestrial weathering in MIL 05035, 6, shown by the reddish brown tarnish color, and the presence of clay minerals, is found in a restricted region along cracks that cut through the fusion crust. Seven sections studied by different groups display a non-uniform distribution of minerals that likely reflects a sectioning effect due to the coarse-grain size (Table 1). Using data from this study and that of Joy et al. (2008), average modal abundances for MIL 05035 were calculated, after correcting for variable polished-section areas (Table 1).

#### *Pyroxene*

Pyroxene is the most abundant mineral in MIL 05035 (Table 1) and occurs mainly as primary grains, as well as secondary grains in symplectite. Secondary pyroxenes in the symplectite assemblages are relatively homogeneous with a composition of  $Wo_{37 \pm 3}En_{11 \pm 2}Fs_{52 \pm 3}$ . Individual primary grains are readily identified with an optical microscope and possess edges that are generally intergrown with maskelynitized plagioclase and symplectite. Most primary pyroxenes are twinned. Compositions of primary pyroxenes (up to 5 mm long) show extensive variations in terms of Ca-Mg-Fe contents, from relatively Fe-poor cores ( $Mg/Fe = 1$ ) that grade toward ferroaugite rims ( $En_3Fs_{56}$ , Table 3, Fig. 2a), and are similar to those reported by Joy et al. (2008). Molar Fe/Mn ratios of the primary pyroxenes (~62) follow a typical lunar trend (e.g., Papike et al. 2003). Correlations of Ti# with Mg# of pyroxenes from our sections coincide with those of Joy et al. (2008) and are also similar to trends defined in A-881757 (Koeberl et al. 1993), but occur at higher Ti# and lower Mg# than the range of pyroxene compositions in Y-793169 (Koeberl et al. 1993) and basaltic clasts of MET 01210 (Day et al. 2006b). The cation Al/Ti ratios from our pyroxenes also overlap with those from Joy et al. (2008), starting at Mg# of 54 and Al/Ti of 3 (Fig. 2). Compared to other lunar basalts and basaltic meteorites (except for A-881757), MIL 05035 pyroxene cores are more Fe-rich (Fig. 2a), and rims lack enrichment toward pyroxferroite, with only a single grain discovered to have this composition (star in Fig. 2a). The compositions of the ferroaugite rims of MIL 05035 pyroxenes are located in the "forbidden zone" of pyroxenes (Fig. 2a) and are, therefore, metastable (Lindsley 1983).

MIL 05035 pyroxenes show complex zonation, which occur throughout the meteorite (Arai et al. 2007; Joy et al. 2007, 2008). Complex zonation is clearly expressed in X-ray maps of individual pyroxenes (e.g., Ca, Fe, Fig. 3). Sector zones of pyroxene were complicated by twins and pervasive thin flames of low-Ca pyroxene. EMP traverses of these pyroxenes (Fig. 4) show nearly constant Mg# ( $52 \pm 2$ ) and Al/Ti (~3), with alternating Ca content in the core region (~1 mm wide). Arai et al. (2007) reported cyclic Wo contents (from pigeonite to augite) with limited variation of Mg# (55–45), which are possibly due to the thin low-Ca veinlets described above. Co-existing augite and pigeonite in the pyroxene cores indicate a crystallization temperature of 1000 to 1100 °C, using the two-pyroxene thermometer (Lindsley 1983). Cores (~25 vol% of the grain) with nearly constant Al/Ti and Mg# are the earliest crystallized phase (Fig. 4). Toward the rims of pyroxene, Al/Ti decreases gradually from 3 to ~1, suggesting co-crystallization of plagioclase. At the edges of some pyroxenes, Al/Ti ratios are constant at ~1, indicating the occurrence of Fe-Ti oxides in the crystallization sequence. These results for the individual pyroxenes concur with observations from other studies (Arai et al. 2007; Joy et al. 2007, 2008).

Rare earth elements (REEs) in pyroxenes analyzed by SIMS overlap with those measured by LA-ICP-MS from Joy et al. (2008), but Fe-poor pyroxene contains slightly lower REE contents, as measured by SIMS (Fig. 5a). MIL 05035 pyroxenes contain typical REE patterns for lunar pyroxenes, with light-REE (LREE) depletion relative to heavy-REE (HREE; Table 6, Fig. 5a). All pyroxenes display negative Eu anomalies that show limited Sm-Eu-Gd variations ( $Eu/Eu^*$  of 0.21 to 0.3), indicative of the low-oxygen fugacity under which the MIL 05035 basaltic melt crystallized. Augites with  $Wo > 20$  have higher REE contents than the coexisting low-Ca augites and pigeonites (Fig. 5a), which is likely caused by the different compatibility of REEs in high Ca augite and pigeonite (McKay et al. 1986). Fe-rich low-Ca pyroxenes have the greatest enrichment in REEs, reflecting incompatibility during progressive crystallization (Fig. 5a). The highest REE contents were measured in the most-fractionated pyroxene ( $En_3Fs_{56}$ ), near a fayalite grain ( $Fa_{98}$ ), whereas pyroxenes in contact with the symplectites have slightly lower REE concentrations (Fig. 5a). The REEs of these primary pyroxenes are similar to pyroxenes in Apollo 15 low-Ti, quartz-normative basalts (Schnare et al. 2008).

#### *Maskelynite*

All plagioclase grains have been converted to maskelynite through impact-related shock processes. A few grains in both sections of MIL 05035, 40 show signs of partial recrystallization (see details in the Shock History section). Maskelynites in MIL 05035 commonly form large clusters (>1 mm long and >0.5 mm wide), with the boundaries

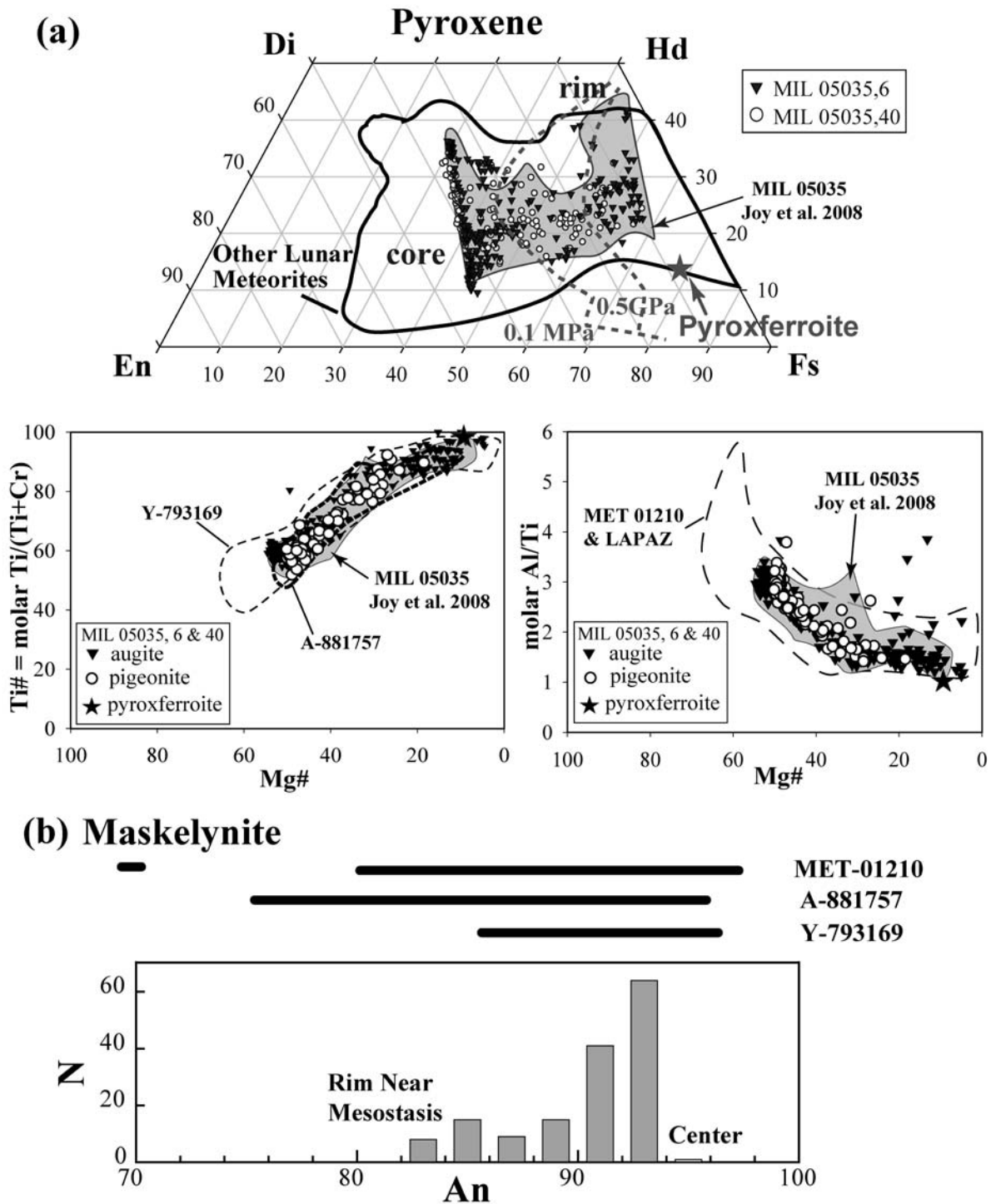


Fig. 2. Pyroxene and plagioclase (maskelynite) mineral compositions for MIL 05035. In (a) only primary pyroxene (excluding pyroxene in symplectites) are plotted. The composition of the pyroxferroite is plotted as star. The shaded fields are MIL 05035 pyroxene from Joy et al. (2008). The outlined field in the pyroxene quadrilateral corresponds to pyroxene compositions measured for other lunar meteorites, e.g., EETA96008 (Anand et al. 2003b), MET 01210 (Day et al. 2006b), LaPaz 02205 and paired stones (Day et al. 2006a; Hill et al. 2009) A-881757 (Koeberl et al. 1993), and Y-793169 (Takeda et al. 1993). Dashed curves in the pyroxene quadrilateral are the "forbidden zone" for 0.1 MPa and 0.5 GPa respectively (Lindsley 1983). In  $Ti\#-Mg\#$  and  $Al/Ti - Mg\#$  plots, open symbols with  $Wo < 20$ , and filled symbols are pyroxenes with  $Wo > 20$ , and open fields include data plotted in Fig. 5 of Joy et al. (2008). b) An contents in maskelynites, compared to A-881757 and Y-793169, and the brecciated, predominantly basaltic meteorite MET 01210. Olivine and plagioclase/maskelynite data in A-881757 and Y-793169 are from Yanai and Kojima (1991) and Takeda et al. (1993), MET 01210 from Day et al. (2006b).

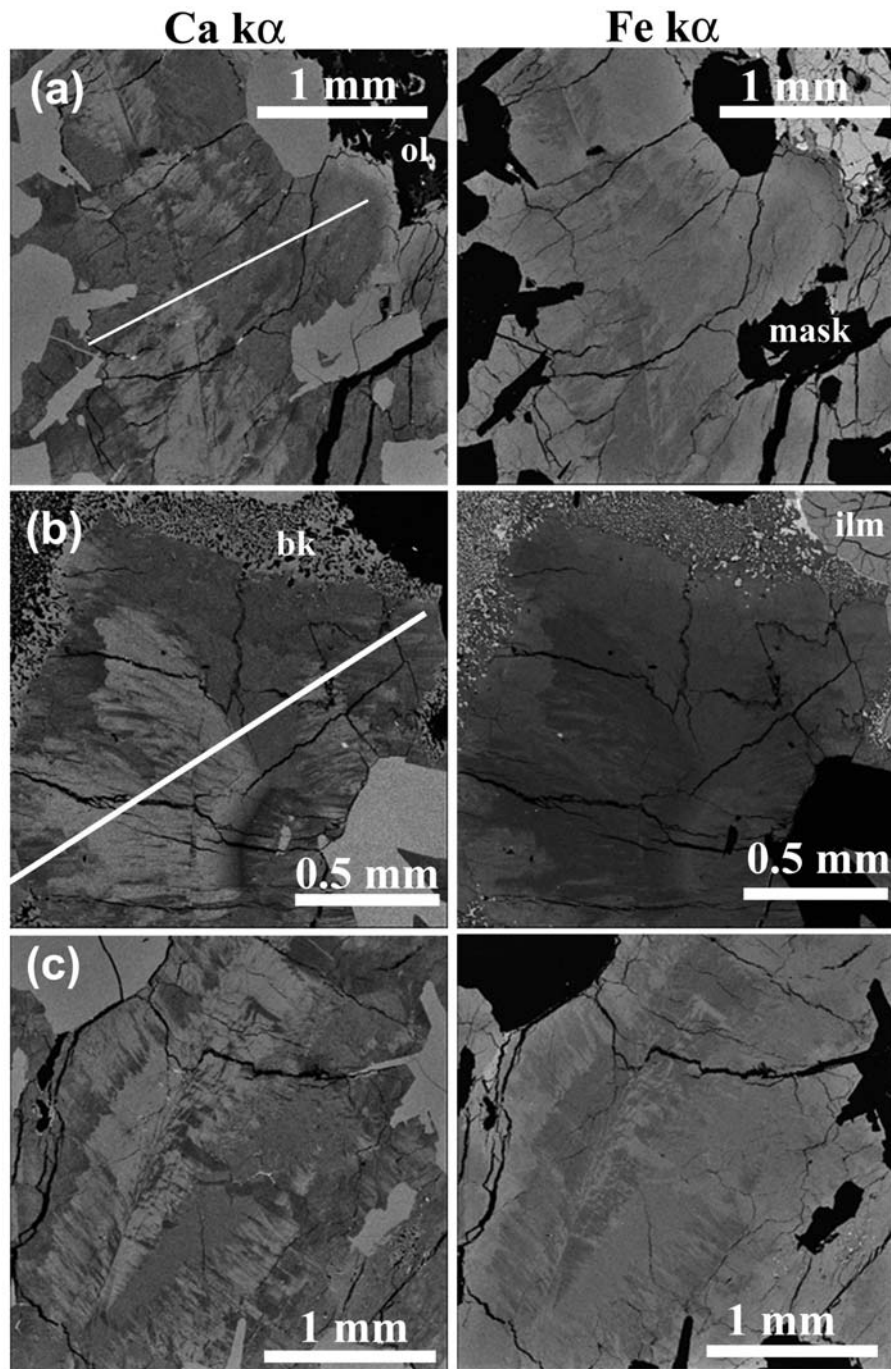


Fig. 3. Complex zoning patterns of pyroxenes in MIL 05035, 6 as shown by Ca  $K\alpha$  and Fe  $K\alpha$  X-ray maps. a) A pyroxene grain in MIL 05035, 6 with sector zoning accentuated by Ca-poor veinlets. b) A pyroxene grain in MIL 05035, 40 with sector zones and twins, containing thin veins of lower Ca, higher Fe pyroxene. White lines in (a) and (b) mark EMPA traverse shown in Fig. 4. c) Complex zoning in a pyroxene grain in MIL 05035, 6 with no clear indication for sector zoning but clear evidence for twinning.

between individual grains in the cluster being routinely defined by submicrometer FeS globules. Smaller grains of maskelynite (<1 mm long; <0.2 mm wide) retain the characteristic lath-shape of primary plagioclase and occur both between and within pyroxenes. Individual maskelynite grains are usually zoned from  $An_{94}$  cores to  $An_{91}$  rims. However, rims in contact with the extremely late-stage

mesostasis are  $An_{83-86}$  (Fig. 2b). Maskelynite with lower An contents ( $An_{77}$  to  $An_{76}$ ) were found in sections studied by Arai et al. (2007) and Joy et al. (2008), implying some degree of heterogeneity within this meteorite. The compositional range of maskelynite grains in MIL 05035 is similar to those in A-881757 and Y-793169 (Koeberl et al. 1993), and in the basaltic clasts of MET 01210 (Day et al. 2006b; Fig. 2b). All

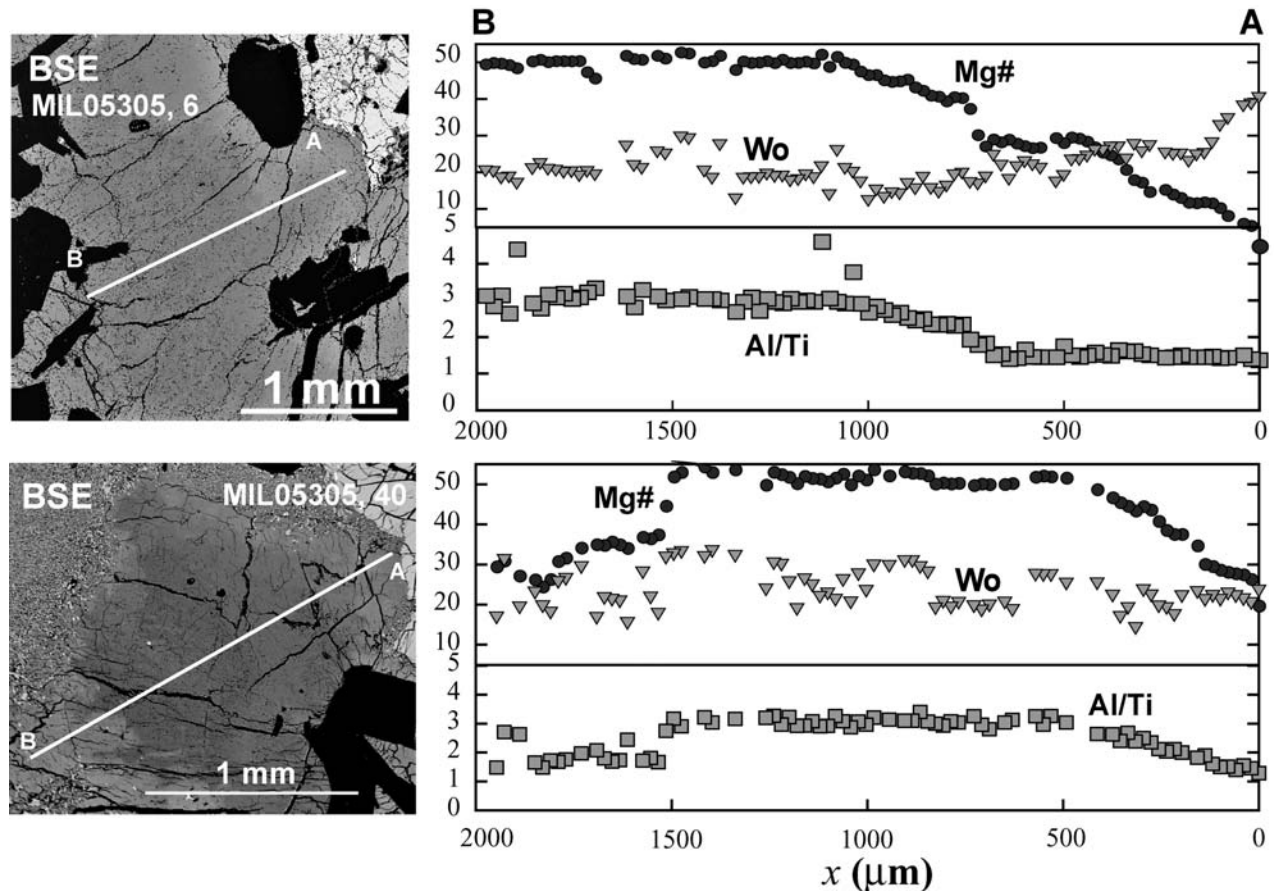


Fig. 4. Compositional variation from center to rim of two pyroxene grains (shown in Fig. 3). EMPA traverses are also plotted on the backscattered electron (BSE) images of the same samples. Al/Ti is the cation ratio of Al and Ti. In the top panel, the Al/Ti ratios is nearly constant at the edge where the pyroxene has a hedenbergite composition. Note the scale change on the y-axis for the plots.

plagioclase grains in A-881757 are maskelynites, whereas plagioclase grains in Y-793169 are recrystallized (Yanai and Kojima 1991; Mikouchi 1999) or partially maskelynitized (Takeda et al. 1993). Trace-element compositions were obtained on traverses from center to rim on some of the maskelynite grains in MIL 05035 (Table 5). The REE concentrations show CI-chondrite normalized patterns typical for lunar plagioclases, with a slightly negative slope, and a strong positive Eu anomaly (Eu/Eu\* of 70–97, Fig. 5b). The REE contents of maskelynites analyzed in our sections lie at the lower end of the total range reported by Joy et al. (2008); as the lower An maskelynite in Joy et al. (2008) has more enriched REE, this is consistent with fractional crystallization.

#### Olivine

Olivines in MIL 05035 are exclusively fayalitic, unlike the majority of Apollo mare basalts. Large (~1 mm) fayalite grains have uniform compositions of Fa<sub>98</sub> (Table 3) and are associated with late-stage phases (SiO<sub>2</sub> droplets, K-Si-rich glass with K-Ba-feldspar [hyalophane], apatite, and baddeleyite) in a “swiss-chess” texture (Fig. 6d), which

suggests that these fayalite grains formed at the extreme end-stage of crystallization, most likely during silicate-liquid immiscibility (Taylor et al. 1971; Anand et al. 2003a). Small fayalitic olivines (Fa<sub>90</sub>, <50 μm) are also found in the mesostasis. Enriched REE contents (CI-normalized values > 1) in large olivine grains from Joy et al. (2008) support the origin of these olivines during late-stage crystallization of the MIL 05035 parental liquid. Secondary olivines occur as ulvöspinel and troilite, with a composition of ~Fa<sub>90</sub>, and as small grains in symplectites with a composition of Fa<sub>94 ± 1</sub>. Similar Fe-rich olivine was found in two other crystalline lunar meteorites: A-881757 and Y-793169, as well as in basalt clasts of the lunar meteorite breccia MET 01210 (Day et al. 2006b). A single fayalite grain (Fa<sub>98.5</sub>) was described from Y-793169 (Yanai and Kojima 1991), whereas fayalitic olivines (Fa<sub>87–95</sub>) were minute-sized grains in symplectites in A-881757 (Yanai 1991).

#### Fe-Ti Oxides

The Fe-Ti oxides (ilmenite and ulvöspinel) were found to be non-uniformly distributed between the two sections studied here (Table 1 and Fig. 7), and among other sections

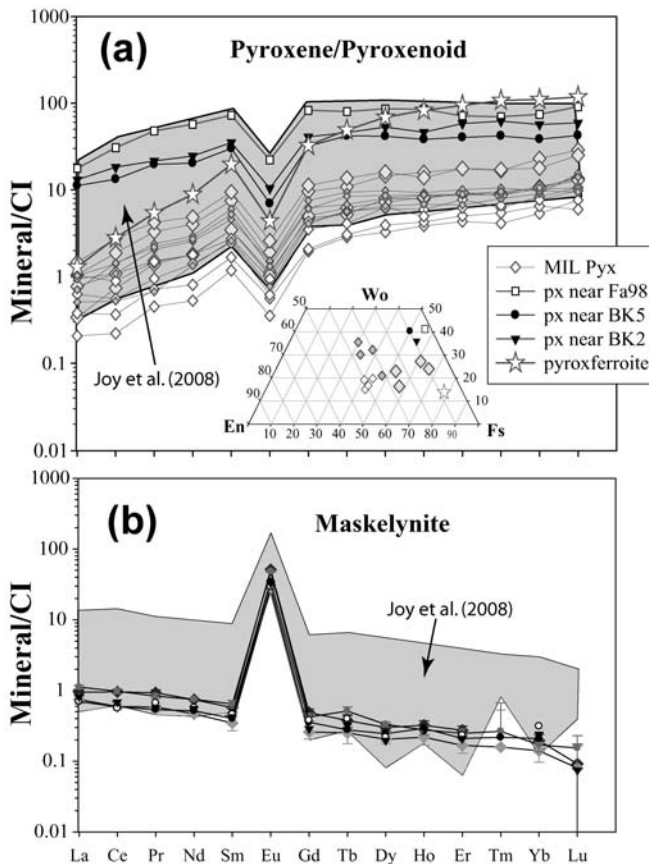


Fig. 5. Rare-earth-element concentrations of minerals normalized to CI chondrite (normalization values from Anders and Grevesse 1989). a) CI-chondrite normalized REE in pyroxenes and a pyroxenoid in MIL 05035. The inset pyroxene quadrilateral corresponds to the major-element compositions of analyzed pyroxenes. b) CI-normalized REE for maskelynite in MIL 05035. Note the broad similarity in compositions to pyroxenes from the LA-ICP-MS study of Joy et al. (2008; shaded areas), but the more elevated REE abundances measured for maskelynites by that study compared with SIMS analyses presented here.

studied by Arai et al. (2007) and Joy et al. (2008). Coarse ulvöspinel occurs as irregular, interstitial grains (Fig. 6c), containing 4.1–7.5 wt%  $\text{Cr}_2\text{O}_3$  and <0.04 wt%  $\text{ZrO}_2$ . These large grains are commonly intergrown with ilmenite and are associated with a fayalitic olivine ( $\text{Fa}_{90}$ ) rim of 20–50  $\mu\text{m}$  thickness (Table 4 and Fig. 6c). The presence of ilmenite and fayalitic olivine is typical for the REEP-fraction of silicate liquid immiscibility, as demonstrated for Luna 24 basalts (Lu et al. 1989). Small irregular ulvöspinel grains are also associated with late-stage mesostasis (Fig. 6a) and are composed of up to 22.6 wt%  $\text{Cr}_2\text{O}_3$  and < 0.05 wt%  $\text{ZrO}_2$  (Table 4 and Fig. 7). Compositions of ulvöspinel grains are similar to many Apollo mare basalts (e.g., Papike et al. 1998) and basaltic clast A in MET 01210 (Day et al. 2006b). Large ilmenites (~1 mm long) appear as interstitial, subhedral to anhedral grains in MIL 05035, 40 (Table 4). One grain in section MIL05035,40 contains a rounded melt inclusion

(~100  $\mu\text{m}$  in diameter). Small ilmenite grains were also observed in the mesostasis in association with baddeleyite and contained detectable  $\text{Cr}_2\text{O}_3$  and  $\text{ZrO}_2$  (0.1–0.4 wt%).

#### Pyroxenoid

A subhedral pyroxenoid grain (~200  $\mu\text{m}$ ), mantled by symplectite (Fig. 8c), occurs in section MIL05035,6. This pyroxenoid has a composition ( $\text{En}_8\text{Fs}_{78}$ ), in the range of lunar pyroxferroite ( $\text{En}_{5-11}\text{Fs}_{76-81}\text{Wo}_{12-13}$ ) reported by Lindsley et al. (1972). The CI-normalized REE pattern in the pyroxenoid is distinctively different from other pyroxenes (Fig. 5a). Because pyroxferroite is an ultra-late-stage liquidus phase, one would expect enriched REE concentrations and a flat REE pattern, similar to that of the ferroaugite (Fig. 5a). However, the steep REE pattern with a fractionated ( $\text{Sm/La}$ )<sub>n</sub> ratio (15) in this grain, compared to other pyroxenes in MIL 05035, suggests that this grain has a different crystal structure from normal pyroxene. We refer to this grain as pyroxferroite in the following discussion, although an exact identification will require a crystallographic determination.

#### Symplectite

MIL 05035 contains a high proportion of symplectites (up to 5.7 vol%) that consist of ferroaugite, fayalite, and a silica phase (Table 1 and Fig. 8). Symplectites of similar mineral assemblages are commonly found in Martian meteorites in similar or lower abundances (e.g., Aramovich et al. 2002). Similar symplectitic intergrowths occur in A-881757 (<5%, Yanai and Kojima 1991; Oba and Kobayashi 2001) and in individual clasts of lunar basaltic breccias (e.g., Anand et al. 2003b; Fagan et al. 2003; Haloda et al. 2005; Fagan 2007), including Clast A of MET 01210 (Day et al. 2006b). Compositions of minerals in symplectites are relatively uniform. Pyroxenes are commonly <50  $\mu\text{m}$  anhedral grains with a uniform composition close to  $\text{Wo}_{37 \pm 3}\text{En}_{11 \pm 2}\text{Fs}_{52 \pm 3}$ ; olivines have  $\text{Fa}_{90}$  compositions (Table 3). Such uniform compositions allow recombination of the bulk composition of symplectites using the volume percentages of minerals and their densities.

Symplectites in MIL 05035 display two main types of textures: a major uniform-distribution and a sub-dominant myrmekitic texture (Figs. 8a–c), and are commonly associated with troilite. Late-stage mesostasis is commonly located near the edges of symplectite. The modal abundances of phases in the symplectites vary between the two main textural types (Table 2), and therefore, affect determination of the bulk compositions of the symplectite. For the uniform-texture symplectite (Fig. 8a), the reconstructed composition (Fig. 8d) lies near the range of lunar pyroxferroite (Lindsley et al. 1972). The symplectite surrounding the pyroxferroite grain featured above has a myrmekitic texture, with a silica phase located at the interface between fayalite and pyroxene (Fig. 8c). However, the mode of ferroaugite, fayalite, and silica of this symplectite is similar to that of the uniform-

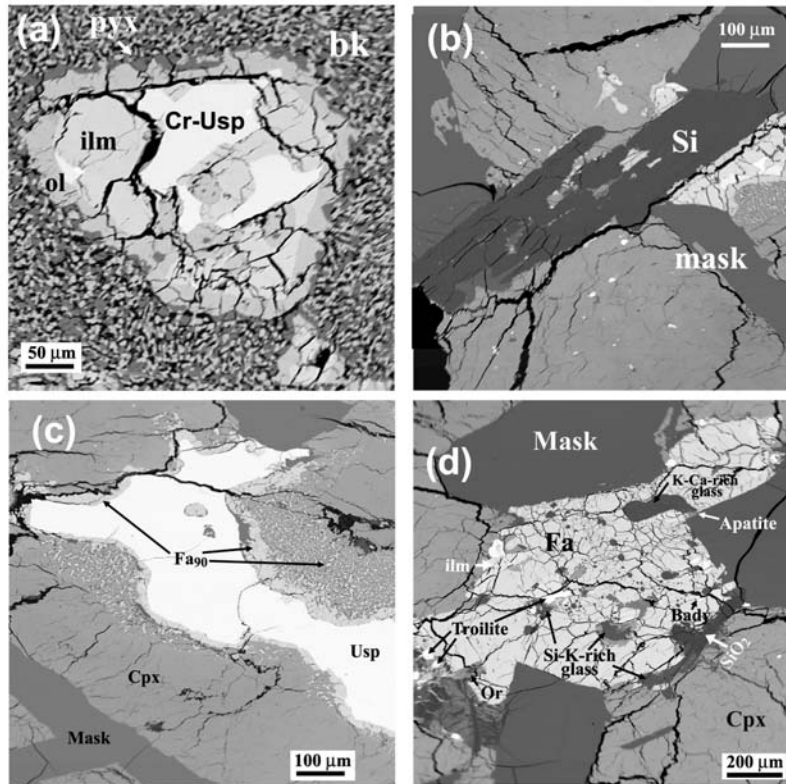


Fig. 6. BSE images of late-crystallizing mineral assemblages in MIL 05035. a) Chromium ulvöspinel (Cr-Usp) is intergrown with ilmenite (ilm), which is rimmed by olivine and surrounded by symplectite in MIL 05305, 40. b) A lath-shaped silica grain (Si) in MIL 05035, 6. c) Anhedrall ulvöspinel in MIL 05035, 6, which possesses a fayalite rim ( $Fa_{90}$ ) and surrounding symplectite regions. d) A large fayalite grain in MIL 05035, 6 with abundant late-stage inclusions. Note the euhedral nature of maskelynitized plagioclase grains surrounding the fayalite grains. Abbreviations are Or-orthoclase, Bady-baddeleyite, Cpx-clinopyroxene, mask-maskelynite, pyx-pyroxene.

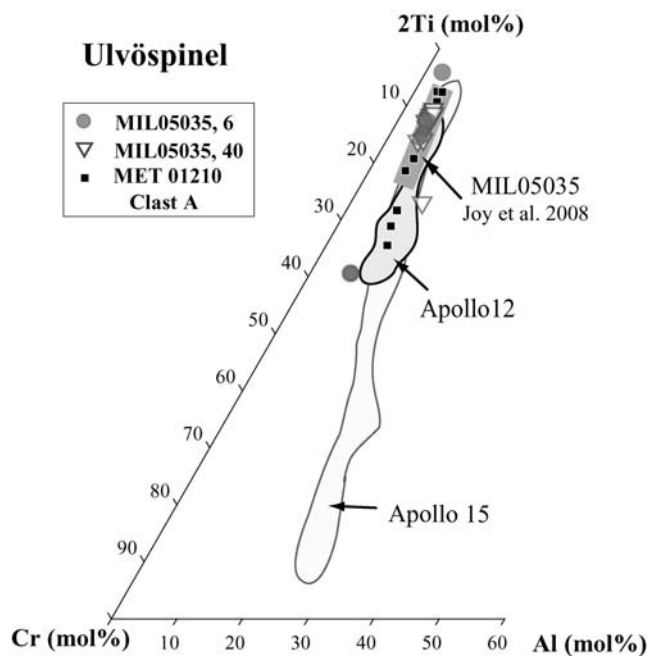


Fig. 7. Compositions of ulvöspinel grains in MIL 05035, in comparison with ulvöspinel in MIL 05035 from Joy et al. (2008) (gray line), in MET 01210 from Day et al. (2006b), and in Apollo low-Ti basalts.

texture type. Therefore, the reconstructed composition also lies in the lunar pyroxferroite range (Table 2). For the other myrmekitic symplectites (Fig. 8b), the reconstructed bulk composition lies in the “forbidden zone” within the pyroxene quad (Fig. 8d), which is similar to the compositions of the rims of primary pyroxene. The above estimates are similar to those measured by broad-beam analyses in A-881757 by Oba and Kobayashi (2001), who used an overly broad electron beam (100  $\mu\text{m}$ ). They reported that bulk compositions are also different: two are near the lunar pyroxferroite field, and the other two are similar to the composition of rims of primary pyroxene.

#### Miscellaneous Phases

The primary silica phase (tridymite?) occurs as long, lath-shaped grains (up to 3 mm, Figs. 1 and 6b), similar to those found in other sections (Joy et al. 2007, 2008). Those silica grains generally are cloudy in the center. A secondary silica phase appears in the symplectites as small grains (<20  $\mu\text{m}$ , Fig. 8). K-rich glass also occurs in the mesostasis and in fayalite, containing 3–10.3 wt%  $\text{K}_2\text{O}$  and <0.9 wt% BaO. A few K-rich and Ba-rich feldspars (Table 3b;  $\text{BaO} \leq 12.2$  wt%,  $\text{K}_2\text{O} \leq 14.5$  wt%) included in fayalite are typical late-stage phases in low-K mare basalts (e.g., Papike et al. 1998), and in

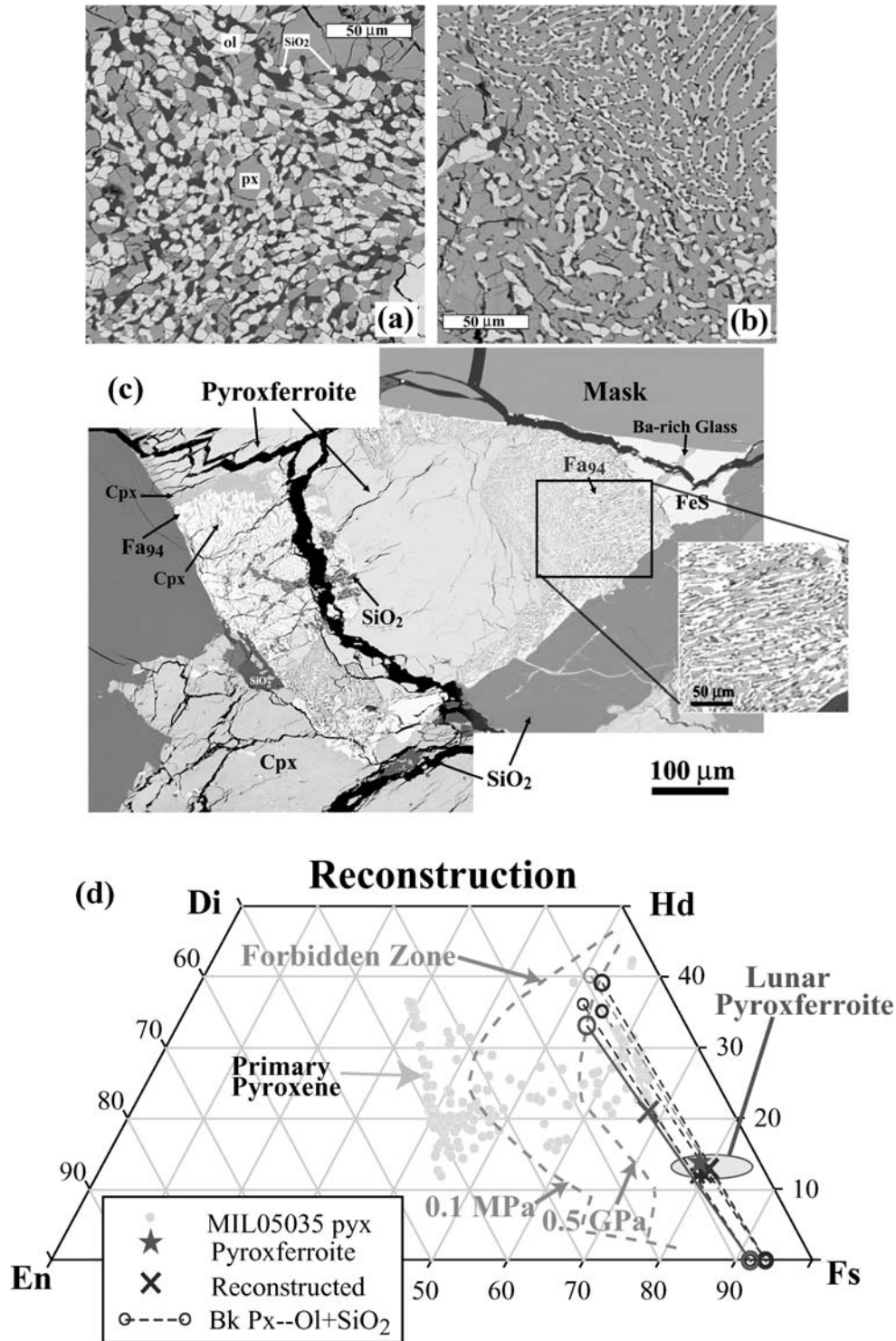


Fig. 8. BSE images of symplectites in MIL 05035, 6. Image (a) shows that breakdown minerals in the assemblage are uniformly distributed. b) Myrmekitic texture with SiO<sub>2</sub> along the boundary between pyroxene and olivine. c) Symplectite are intimately associated with pyroxferroite. Square outlines the area used for reconstructing the bulk composition of the myrmekitic symplectite. d) Reconstructed composition of breakdown assemblage. Light filled symbols are primary pyroxene, star is the pyroxferroite grain. Tie lines connects pyroxene in the symplectite and “ferrosilite” (fayalite + SiO<sub>2</sub>). Crosses on the tie line are reconstructed compositions. The ellipse is the composition of lunar pyroxferroite (Lindsley et al. 1972). Dashed curves are the boundary of the “forbidden zone” (Lindsley 1983), to the right of which pyroxenes are unstable.

MIL 05035, they are associated with troilite and fayalite. Troilite (FeS) occurs as small (<200  $\mu\text{m}$ ) irregular grains near or in symplectites or as small (<1–2  $\mu\text{m}$ ) globules inside maskelynite. Apatite is present as euhedral grains (<100  $\mu\text{m}$ ) with variable F (1.4–2.3 wt%) and Cl (0.19–0.95 wt%) contents. Trace amounts of baddeleyite are included in fayalite.

### Bulk Rock Compositions

The coarse-grained nature of MIL 05035 requires a large amount of sample for a representative bulk rock analysis, as suggested previously for other coarsely crystalline mare basalts (e.g., Ryder and Schuraytz 2001). Previous studies on MIL 05035 have already demonstrated compositional variation in bulk rock compositions, due to the coarse-grain size (Arai et al. 2007; Joy et al. 2007, 2008; Korotev and Zeigler 2007). In addition, the highly zoned nature of pyroxene, the most abundant phase in the rock, contributes considerable imprecision to the modal recombination calculations using mineral modes and average mineral compositions (Liu et al. 2007). The bulk rock composition reported here was obtained on a larger amount of sample (aliquot from a 1.9 g well-homogenized sample powder) than that used by Joy et al. (2007, 2008; aliquot from ~0.31 g chip). These two measurements differ slightly in major-element compositions but have similar trace-element compositions (Table 7). The only differences, in terms of trace elements, between the two datasets occur for Cu and Zn, which are at lower concentrations in our measurements of MIL 05035, and Ge and W, which have more elevated abundances in our analysis (possible contamination from the Mo strip heater during fusion). The new data presented here indicate that MIL 05035 is a “low-Ti” type mare basalt according to the classification scheme of Neal and Taylor (1992), and are in good agreement with previous work (Fig. 9). The CI-normalized REE patterns of MIL 05035 from our study are similar to those presented in Joy et al. (2007, 2008), displaying a moderately LREE-depleted profile with  $(\text{La}/\text{Sm})_n = 0.63$  and  $(\text{La}/\text{Yb})_n = 0.44$  (Fig. 10). Compared with other low-Ti to very-low-Ti lunar mare basalts (Y-793169 and A-881757) and basaltic breccia meteorites (MET 01210), MIL 05035 is more depleted in incompatible elements.

## DISCUSSION

### Shock History of MIL 05035 and the Origin of Symplectite in Achondrite Meteorites

Abundant shock features were found in our sections of MIL 05035, as well as reported in other studies of this meteorite (Arai et al. 2007; Joy et al. 2007, 2008; Liu et al. 2007; Zeigler et al. 2007). In all cases, plagioclase has been

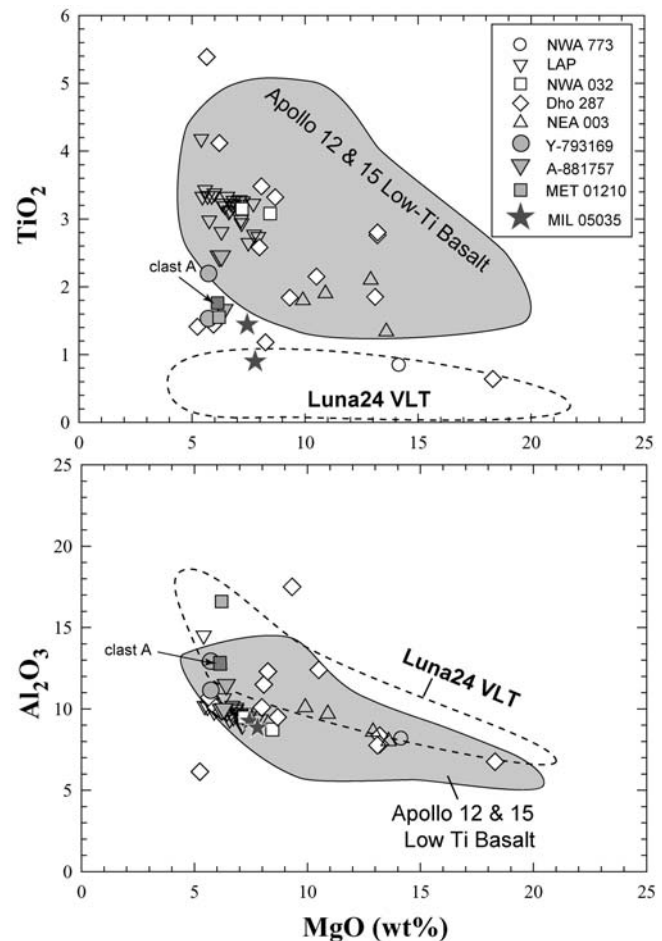


Fig. 9. Bulk rock chemistry of MIL 05035 in comparison with other low Ti lunar basalts. Data sources are MIL 05035: this study and Joy et al. (2008), Apollo 12 and 15 low-Ti, and Luna 24 VLT basalts: Mare Basalt Database by C. Neal (<http://www.nd.edu/~cneal/Lunar-L/>); Lunar mare basaltic meteorites: Lunar Meteorite Compendium by K. Righer (<http://www-curator.jsc.nasa.gov/antmet/lmc/index.cfm>).

completely converted to maskelynite, suggesting shock pressures above 30 GPa (Stöffler et al. 1991) and at the upper end of the vitrification range (30–45 GPa, Ostertag 1983). A few maskelynite grains show signs of the initiation of recrystallization (Fig. 11). Submicron troilite grains follow sealed fracture planes/grain boundaries in maskelynite (Fig. 11). Stöffler et al. (1991) found that melting and mobilization of sulfide phases occurred in olivine in ordinary chondrites that display mosaicism and planar-deformation features (PDF), corresponding to shock pressures of >30–35 GPa. Shock-induced melting in other sections, reported by Arai et al. (2007), suggests localized heating at >45 GPa. Planar-deformation features in a primary silica phase, similar to those reported in Fig. 4 of Joy et al. (2008), were also observed in our sections, indicating shock pressures of 8–25 GPa (French 1998). Pyroxenes contain fractures (irregular and planar),

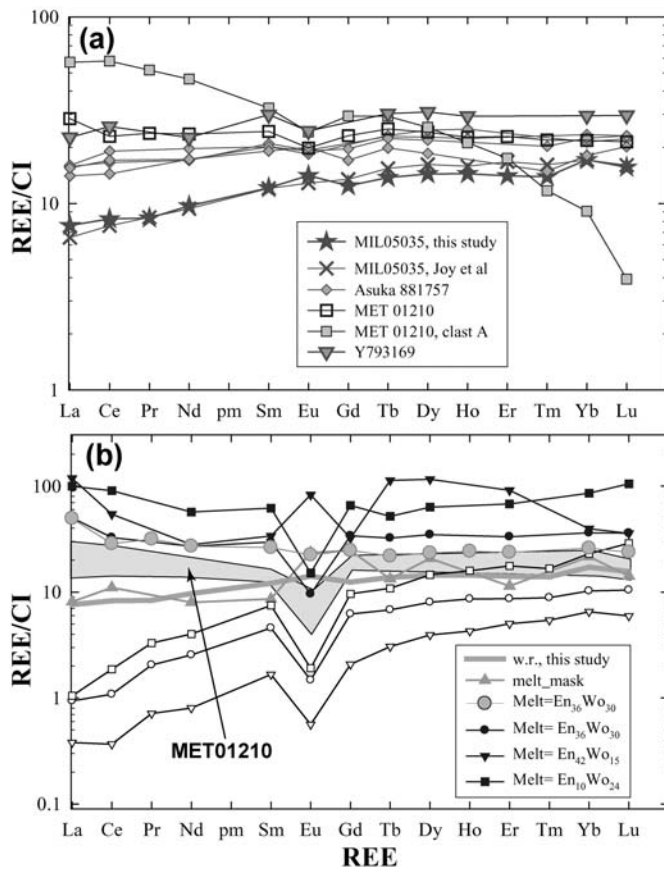


Fig. 10. CI-normalized rare earth element patterns for MIL 05035 versus calculated melt compositions (normalization values from Anders and Grevesse 1989). a) Bulk rock REEs of MIL 05035 are compared to other studies: whole rock of MIL 05035 (Joy et al. 2007, 2008), paired meteorites of A-881757 (Warren and Kallemeyn 1993; Koeberl et al 1993), Y-793169 (Warren and Kallemeyn 1993), and MET 01210 (Joy et al. 2006a). b) CI-normalized REEs of melts equilibrating with MIL 05035 pyroxenes and plagioclase. REEs of pyroxenes (open symbols) and bulk rock MIL 05035 (thick gray lines) are plotted for comparison. Calculated melts using partition coefficients from McKay et al. (1986, 1991) are small solid symbols, and that for an augite (En<sub>36</sub>Wo<sub>30</sub>) using Schnare et al. (2008) are large filled circles. The melt equilibrating with maskelynite (An<sub>92</sub>) was calculated using partition coefficients for plagioclase from Phinney and Morrison (1990). The field in (b) are melt equilibrating with early pyroxenes in MET 01210 from Day et al. (2006b).

dislocations, undulatory extinction, PDF and possible mosaicism (Figs. 11a and 11b). The PDF reflect shock pressures of 25–80 GPa (Stöffler et al. 1991), whereas the mosaicism of pyroxenes involves pressures of 30–75 GPa (Schaal et al. 1979). Similar PDF in other sections were reported by Joy et al. (2008). We conclude that this meteorite was strongly shocked (S5 stage using the terminology of Stöffler et al. [1991]), with signs of localized heating/melting.

Meteorites derived from the Moon and Mars that contain symplectite breakdown textures are typically highly shocked (e.g., Yanai and Kojima 1991; Aramovich et al. 2002).

Although the symplectic intergrowth feature of ferroaugite, fayalite, and SiO<sub>2</sub> has commonly been interpreted as the breakdown of pyroxferroite due to slow cooling (e.g., Oba and Kabayashi 2001; Aramovich et al. 2002), it may not be coincidental that these meteorites have also suffered intense shock. An important textural observation for MIL 05035 is the presence of incomplete breakdown of pyroxferroite (Fig. 8c), and there are textural and chemical differences within the symplectite assemblages of MIL 05035 (Fig. 8). These petrologic features point to decomposition of pyroxferroite and metastable ferro-hedenbergites that was fast, incomplete, insensitive to chemistry, and selective of interface and structure within the sample. Shock-induced heat is consistent with these observations, as it generally dissipates (cools) fast and is controlled by structure (Stöffler et al. 1991). Therefore, it is also possible that the breakdown of pyroxferroite in other achondrite meteorites may be a function of shock rather than slow cooling on their parent body.

#### Cooling Rate and Crystallization History of MIL 05035

There are several developed geospeedometers including Fe-Mg diffusion in olivine (e.g., Taylor et al. 1977) and Zr diffusion between ilmenite and ulvöspinel (Taylor et al. 1975). The Fe-Mg diffusion method is not applicable because olivines in MIL 05035 are only fayalitic and homogeneous. The coarse grain size of MIL 05035 limits the usefulness of crystal size distribution (CSD) techniques as the number of crystals in the limited surface area of a thin section make any analysis using this technique statistically suspect. Using Zr contents 10–15  $\mu\text{m}$  from the ulvöspinel-ilmenite contact in coarse grains (0.02–0.03 wt% ZrO<sub>2</sub> for ulvöspinel, 0.07–0.08 wt% for ilmenite), and the method in Taylor et al. (1975), a cooling rate of 0.7 to 3  $^{\circ}\text{C}/\text{h}$  was obtained. Touching ulvöspinel-ilmenite pairs in mesostasis yield unreasonably high temperature (>1400  $^{\circ}\text{C}$ ), suggesting possible subsolidus reactions. The cooling rate of MIL 05035 can be roughly estimated using the size of pyroxene and the experimental data on low-Ti mare basalt by Grove and Walker (1977). The width of (110) section of a few pyroxene grains (1–2 mm) yields a rate of  $\sim 0.2\text{--}0.4$   $^{\circ}\text{C}/\text{hr}$ . We caution that these rates and the size of the pyroxene grains are outside the experimental ranges in Grove and Walker (1977). The presence of pyroxferroite grains can also be used to estimate the cooling rate in conjunction with crystallization temperature estimates of Fe-poor pyroxene cores (1000–1100  $^{\circ}\text{C}$ ). The experiments from Lindsley et al. (1972) state that pyroxferroite is stable if cooled to <990  $^{\circ}\text{C}$  in 3 days from crystallization. Considering pyroxferroite to be an ultra-late-stage phase during crystallization, and using 1000  $^{\circ}\text{C}$  as its crystallization temperature, we calculate a cooling rate of  $\sim 0.2$   $^{\circ}\text{C}/\text{h}$ , which is in close agreement with the Zr-diffusion and pyroxene width data. These estimates are, perhaps, the minimum limit of the

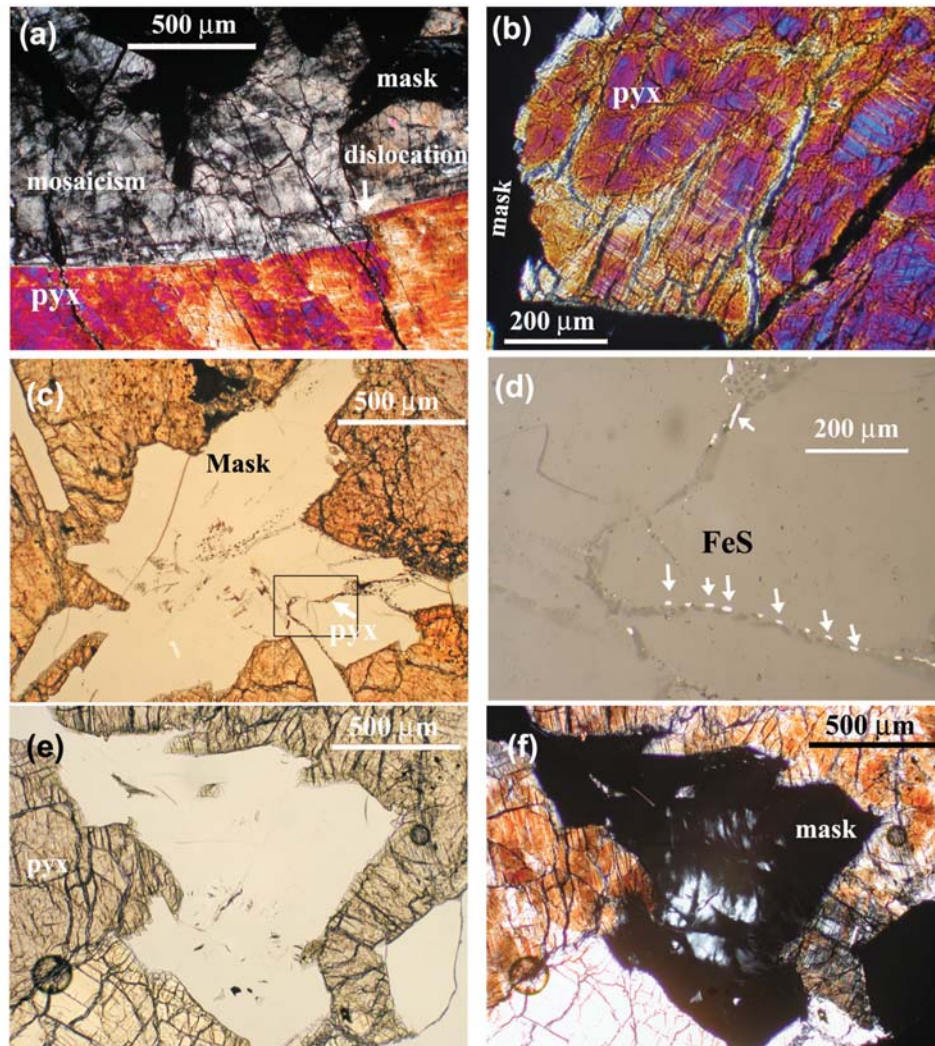


Fig. 11. Shock features in MIL 05035. a) Cross-polar transmitted-light image of pyroxene twins. Note the dislocation on the twinning plane. One twin displays a mosaic extinction pattern, whereas the other shows planar deformation features. b) Cross-polar transmitted-light image of a pyroxene with an abundance of planar deformation features. c) Transmitted light image of maskelynite. The box outlines the area imaged in (d). d) Reflective light image of maskelynite with trains of FeS globules lining the grain boundary or sealed fractures. e) Transmitted light image and f) cross-polar image of partially recrystallized maskelynite grains.

cooling rate for MIL 05035. Using the width of plagioclase grains and experimental curve of plagioclase of Grove and Walker (1977), Joy et al. (2008) obtained a rate of 0.07 °C/h for MIL 05035. Our observations of plagioclase in MIL 05035 are that they normally form as clumps or clusters, and therefore, using the width of these clusters may underestimate the cooling rate. The cooling rate estimate of ~0.2 °C/h is broadly consistent with Luna 24 basalts (Grove 1978) and implies crystallization within a lava flow with a thickness of ~10–20 m (Grove and Walker 1977).

Petrography and mineral chemistry suggest that MIL 05035 crystallized in the sequence:

Fe-poor pigeonite and augite → Fe-rich augite + plagioclase ± ulvöspinel → hedenbergite + ulvöspinel ± ilmenite late-stage mesostasis.

Theoretical modeling using MELTS was attempted, but failed to yield mineral compositions consistent with those observed in MIL 05035. This is likely due to the fact that MELTS fails to reproduce crystallization sequences at low  $fO_2$  conditions (IW) (Slater et al. 2003; Thompson et al. 2003). MAGPOX/MAGFOX software (Longhi 1991, 2002), while successful at  $fO_2 \sim IW$ , produced olivine on the liquidus ( $FO_{63}$ ), and thus could not be used for modeling of MIL 05035.

The crystallization of MIL 05035 can be further examined by comparing trace-element compositions of estimated parental melts from mineral compositions with the measured bulk rock composition. The parental melt in equilibrium with pyroxenes was calculated using distribution coefficients for La-Sm, Yb, and Lu interpolated to their corresponding Wo number using the equation from McKay

et al. (1986), and Eu, Tb, Dy, and Er from McKay et al. (1991). Partition coefficients for augites were also obtained on an Apollo 15 quartz-normative basalt (15499), which possesses a vitrophyric (glassy) matrix texture (Schnare et al. 2008). We used values for  $Wo_{31.7}$  pyroxenes from Schnare et al. (2008) to estimate parental melts for the early crystallized  $Wo_{30}$  pyroxene ( $Mg\# = 51.4$ ) in MIL 05035. Distribution coefficients for REE in plagioclase are taken from Phinney and Morrison (1990). The estimated parental melts for early, coexisting Fe-poor pyroxene cores ( $Wo_{15}$  and  $Wo_{30}$ ), using McKay et al. (1986, 1991), have broadly similar REE patterns (Fig. 10), which indicates that the early formed pyroxenes originated from a single-melt composition. Relative enrichment of these estimated parental-melt compositions likely reflect uncertainty in partition coefficients, rather than any petrogenetic effect. This is demonstrated by the similarity of REEs between calculated melt, using the “natural” partition coefficients from Schnare et al. (2008), and the measured bulk rock (Fig. 10). The REE patterns of the estimated melts from early formed maskelynite are also similar to the bulk rock composition with a weak positive Eu anomaly. By contrast, the estimated-melt composition equilibrating with more evolved pyroxenes ( $En_{10}Wo_{24}$ ) is somewhat enriched with respect to Fe-poor pyroxenes, indicating fractionation of the parental melt, most likely within the lava flow. Thus, the crystallization and cooling history of MIL 05035 is consistent with generation from an incompatible element-depleted parental melt that underwent fractionation during early cooling and crystallization, probably of olivine ( $\pm$ spinel), most likely during lava flow or shallow-level emplacement, to generate the MIL 05035 parental liquid.

### Crater Source Pairing with Y-793169 and A-881751

Among over 130 lunar meteorites found worldwide to date, MIL 05035 is one of only 10 mare basalt meteorites. These types of lunar meteorites range from low-Ti to very-low-Ti basalts and are likely under-represented in the Apollo and Luna samples given the global variation in  $TiO_2$  abundances for the Moon (Giguere et al. 2000). Among these lunar mare basalt meteorites, MIL 05035 shows the closest affinity to A-881751 and Y-793169. The similarities extend to mineralogical and bulk major- and trace-element compositions, radiogenic isotope characteristics, and ages that range between 3.7 to 3.9 Ga (Yanai 1991; Yanai and Kojima 1991; Misawa et al. 1992; Takeda et al. 1993; Oba and Kobayachi 2001; Nyquist et al. 2007). Like Joy et al. (2008), we suggest that MIL 05035 is most likely source crater-paired with Y-793169 and A-881751.

Joy et al. (2008) also proposed that MIL 05035 was likely launch-paired with the immature, predominantly basaltic, glassy-matrix regolith breccia, MET 01210, based on basaltic clasts within that rock (e.g., Clast A; Day et al. 2006b). They

argued that the  $3.90 \pm 0.09$  Ga age for basaltic clasts in MET 01210 (Terada et al. 2007), the cosmic ray exposure age of  $0.9 \pm 0.2$  Ma for MET 01210 (Nishiizumi et al. 2006), and the bulk composition of MET 01210 are similar to those of A-881757 and Y-793169 (Arai et al. 2005), which were all evidence for launch-pairing. Day et al. (2006b) demonstrated that a variety of clasts exist within MET 01210, including agglutinate, anorthosite and basalt clasts, some of which are similar in composition to MIL 05035 (e.g., Clast A), and some of which are not (e.g., Clasts AA, K). Importantly, a number of these clasts contain pyroxenes that are more Mg-rich than the most magnesian in MIL 05035 (Fig. 2 of Day et al. 2006b). Furthermore, given the polymict nature of MET 01210, its bulk rock composition likely reflects a complex amalgamation of materials rather than a simple melt composition.

Based on these arguments above, MET 01210 can, at best, be considered launch-paired with MIL 05035, Y-793169, and A-881757 and certainly bears little relation to these meteorites in terms of a lava flow/regolith model (Fig. 11 of Joy et al. 2008), although clasts within MET 01210 may be related to those meteorites. MIL 05035, Y-793169, and A-881757 can be linked in a manner similar to that originally proposed by Day and Taylor (2007). Given the differences in grain size and incompatible trace element concentrations (c.f. Fig. 10a), this likely reflects crystallization within a lava flow with a stratigraphy corresponding to MIL 05035 and A-881757 near the center of the flow and Y-793169 near the top or at the chilled base.

### Implications for the Origin and Mantle Source of MIL 05035

Y-793169, A-881757, and MIL 05035 form a group of low-Ti basalts that are relatively rich in Fe and have older ages (3.7–3.9 Ga) than other low-Ti lunar basalts ( $<3.4$  Ga; e.g., Anand and Terada 2008). Nyquist et al. (2007) have presented isotopic evidence for similarities between A-881757 and MIL 05035, and showed that initial  $^{87}Sr/^{86}Sr$  and  $^{143}Nd/^{144}Nd$  compositions for MIL 05035 were consistent with an incompatible and LREE-depleted mantle source composition. The bulk rock trace element composition for MIL 05035 [ $(La/Sm)_n = 0.63$  and  $(La/Yb)_n = 0.44$ ] is also consistent with a LREE-depleted parental melt (Table 7 and Fig. 10a). Based on these arguments, Nyquist et al. (2007) preferred an origin of MIL 05035, A-881757 and, by inference, Y-793169, in the pre-Nectarian Australe basin or Mare Humboldtianum. Joy et al. (2008) argued for similar regions, as well as Mare Humorum. Certainly these meteorites are unlikely to have originated from the Th-rich Procellarum KREEP Terrane (Jolliff et al. 2000).

The incompatible element-depleted composition of MIL 05035 need not reflect fractional crystallization of this basalt given Sr and Nd isotope evidence for mantle source depletion.

However, the relatively low MgO content (7.5 wt%) and presence of only pyroxene and plagioclase on the liquidus suggests that some degree of crystal-liquid fractionation has occurred to generate the MIL 05035 bulk rock composition. Nevertheless, it appears that MIL 05035 (and A-881757 and Y-793169) originate from a depleted lunar-mantle source. Lunar mare basalts are considered to derive from a strongly differentiated lunar mantle that was most likely generated via a magma ocean event (Warren 1985, and references therein). In this model, differentiation would lead initially to generation of orthopyroxene- and olivine-rich cumulates, with plagioclase appearing on the magma ocean liquidus after as much as 78% magma ocean crystallization, with KREEP forming even later (Snyder et al. 1992). Early-formed cumulates would thus be characterized by a depleted incompatible element inventory and a lack of Eu anomaly, that is otherwise so pervasive in PKT-derived basalts, such as the Apollo 15 basalts (e.g., Schnare et al. 2008).

It is highly probable that MIL 05035 was derived from a fractionated melt derived from a depleted source on the Moon. The ages of MIL 05035, as well as A-881757 and Y-793169 (3.7–3.9 Ga) imply melting of this source prior to Apollo-sampled, high-Ti mare basalt (3.6–3.8 Ga) or low-Ti mare basalt magmatism (<3.4 Ga; Nyquist and Shih 1992). The maximum ages also coincide with the prevalent age data for lunar impact-melt rocks (Norman et al. 2006). A possible mechanism to melt early formed lunar cumulate mantle to generate MIL 05035 would be impact-derived adiabatic decompression or heating, although this model requires careful assessment. Alternatively, the more enriched incompatible-element characteristics of later mare basalt magmatism may reflect the onset of mantle overturn in the Moon (e.g., Day et al. 2006c).

### SUMMARY

MIL 05035 is a low-Ti mare basalt, consisting predominantly of coarsely crystalline pyroxene and maskelynite. Pyroxene compositions are slightly more Fe-rich (Mg# <50) than those typical for low-Ti mare basalts. All plagioclase crystals were shocked to maskelynite, which is commonly zoned from An<sub>94</sub> to An<sub>91</sub>. Lower An contents (An<sub>84</sub>) were found in direct contact with late-stage minerals and mesostasis. The chemical zoning in MIL 05035 pyroxenes suggest the most Mg-rich pyroxene crystallized before plagioclase. Ulvöspinel and ilmenite are late-crystallizing phases formed together with hedenbergite and fayalite.

Symplectites, as intergrowths of fayalite, silica, and Fe-rich augite, are formed by breakdown of Fe-rich pyroxene and pyroxferroite. Different textures and bulk compositions of symplectites, as well as the incomplete decomposition of pyroxferroite, indicate they were formed by shock-induced, localized heating as supported by melt pockets, shock features in silica, and mobilization of troilite.

Based on petrography, major- and trace-element chemistry of the whole rock and minerals, and Sm-Nd and Rb-Sr isotope evidence (Nyquist et al. 2007), MIL 05035 appears to be source crater-paired with A-881757 and Y-793169. These meteorites form a group of 3.7–3.9 Ga mare basalts characterized by coarse-grain size, low-Ti, high-Fe, and relatively depleted incompatible elements including the REE. These features reflect melting of a source region that consisted mainly of olivine and pyroxene in the lunar mantle.

*Acknowledgments*—We thank MWG for provision of portions of MIL 05035 for mineralogical and petrological study and Allan Patchen for assistance with electron microprobe analyses. The constructive reviews of Mahesh Anand, Kevin Righter, and Allan Treiman, and especially the editorial guidance from Cyrena Goodrich, are greatly appreciated. This research has been supported through NASA Cosmochemistry Grant NNG05GG03G with additional funding provided by the Planetary Geosciences Institute at the University of Tennessee.

*Editorial Handling*—Dr. Cyrena Goodrich

### REFERENCES

- Alexander C. M. O'D. 1994. Trace element distributions within ordinary chondrite chondrules: Implications for chondrule formation conditions and precursors. *Geochimica et Cosmochimica Acta* 58:3451–3467.
- Anand M. and Terada K. 2008. Timing and duration of mare basalt magmatism: Constraints from lunar samples (abstract #2155). 39th Lunar and Planetary Science Conference. CD-ROM.
- Anand M., Taylor L. A., Misra K. C., Demidova S. I., and Nazarov M. A. 2003a. KREEPy lunar meteorite Dhofar 287A: A new lunar mare basalt. *Meteoritics & Planetary Science* 38:485–499.
- Anand M., Taylor L. A., Neal C. R., Snyder G. A., Patchen A., Sano Y., and Terada K. 2003b. Petrogenesis of lunar meteorite EET 96008. *Geochimica et Cosmochimica Acta* 67:3499–3518.
- Anders E. and Grevesse N. 1989. Abundances of the elements: Meteoritic and solar. *Geochimica et Cosmochimica Acta* 53:197–214.
- Antarctic Meteorite Newsletter. 2006. 29(2). p. 37.
- Arai T., Misawa K., and Kojima H. 2005. A new lunar meteorite MET 01210: Mare breccia with a low-Te ferrobasalt (abstract # 2361). 36th Lunar and Planetary Science Conference. CD-ROM.
- Arai T., Misawa K., and Kojima H. 2007. Lunar meteorite MIL 05035: Mare basalt paired with Asuka-881757 (abstract #1582). 38th Lunar and Planetary Science Conference. CD-ROM.
- Aramovich C. J., Herd C. D. K., and Papike J. J. 2002. Symplectites derived from metastable phases in Martian basaltic meteorites. *American Mineralogist* 87:1351–1359.
- Day J. M. D. and Taylor L. A. 2007. On the structure of mare basalt lava flows from textural analysis of the LaPaz Icefield and Northwest Africa 032 lunar meteorites. *Meteoritics & Planetary Science* 42:3–17.
- Day J. M. D., Taylor L. A., Floss C., Patchen A. D., Schnare D. W., and Pearson D. G. 2006a. Comparative petrology, geochemistry, and petrogenesis of evolved, low-Ti lunar mare basalt meteorites from the LaPaz Icefield, Antarctica. *Geochimica et Cosmochimica Acta* 70:1581–1600.

- Day J. M. D., Floss C., Taylor L. A., Anand M., Patchen A. D. 2006b. Evolved mare basalt magmatism, high Mg/Fe feldspathic crust, chondritic impactors, and the petrogenesis of Antarctic lunar breccia meteorites Meteorite Hills 01210 and Pecora Escarpment 02007. *Geochimica et Cosmochimica Acta* 70:5957–5989.
- Day J. M. D., Nowell G. M., Norman M. D., Pearson D. G., Chertkoff D. G., and Taylor L. A. 2006c. Evidence for age-progressive melting of increasingly incompatible-element-enriched mantle reservoirs on the Moon (abstract #2235). 37th Lunar and Planetary Science Conference. CD-ROM.
- Day J. M. D., Pearson D. G., and Taylor L. A. 2007. Highly siderophile element constraints on accretion and differentiation of the Earth-Moon system. *Science* 315:217–219.
- Fagan T. J. 2007. Formation of symplectic inclusions by direct quenching of a high-FeO/(FeO+MgO) silicate liquid on the Moon (abstract). 31st Symposium on Antarctic Meteorites. pp. 15–16.
- Fagan T. J., Taylor G. J., Keil K., Hicks T. L., Killgore M., Bunch T. E., Wittke J. H., Mittlefehldt D. W., Clayton R. N., Mayeda T. K., Eugster O., Lorenzetti S., and Norman M. D. 2003. Northwest Africa 773: Lunar origin and iron-enrichment trend. *Meteoritics & Planetary Science* 38:529–554.
- Fernandes V. A., Morris A., and Burgess R. 2005. New Ar-Ar age determinations for the lunar mare basalts Asuka-881757 and Yamato-793169 (abstract #1002). 36th Lunar and Planetary Science Conference. CD-ROM.
- Floss C., James O. B., McGee J. J., and Crozaz G. 1998. Lunar ferroan anorthosite petrogenesis: Clues from trace element distributions in FAN subgroups. *Geochimica et Cosmochimica Acta* 62:1255–1283.
- French B. M. 1998. *Traces of catastrophe: A handbook of shock-metamorphic effects in terrestrial meteorite impact structures*. LPI Contribution 954. Houston: Lunar and Planetary Institute. 120 p.
- Giguere T., Taylor G. J., Hawke B. R., and Lucey P. G. 2000. The titanium contents of lunar mare basalts. *Meteoritics & Planetary Science* 35:193–200.
- Grove T. L. and Walker D. 1977. Cooling histories of Apollo 15 quartz-normative basalts. Proceedings, 8th Lunar Science Conference. pp. 1501–1520.
- Haloda J., Irving A. J., and Tycova P. 2005. Lunar meteorite Northeast Africa 001: An anorthositic regolith breccia with mixed highland/mare component (abstract #1487). 36th Lunar and Planetary Science Conference. CD-ROM.
- Hill E., Taylor L. A., Floss C., and Liu Y. 2009. LaPaz 04841: petrology, texture, and impact-shock effects of a low-Ti mare basalt. *Meteoritics & Planetary Science* 44:87–94.
- Hsu W. 1995. Ion microprobe studies of the petrogenesis of enstatite chondrites and eucrites. Ph.D. thesis, Washington University, USA.
- Jolliff B. L., Gillis J. J., Haskin L. A., Korotev R. L., and Wiezorek M. A. 2000. Major lunar crustal terranes: Surface expressions and crust-mantle origins. *Journal of Geophysical Research* 105: 4197–4216.
- Joy K. H., Anand M., Crawford I. A., and Russell S. S. 2007. Petrography and bulk composition of Miller Range 05035: A new lunar VLT gabbro (abstract #1867). 38th Lunar and Planetary Science Conference. CD-ROM.
- Joy K. H., Crawford I. A., Anand M., Greenwood R. C., Franchi I. A., and Russell S. S. 2008. The petrology and geochemistry of Miller Range 05035: A new lunar gabbroic meteorite. *Geochimica et Cosmochimica Acta* 72:3822–3844.
- Koeberl C., Kurat G., and Brandstätter F. 1993. Gabbroic lunar meteorites Asuka-881757 (Asuka-31) and Yamato-793169: Geochemical and mineralogical study. *Proceedings of the NIPR Symposium on Antarctic Meteorites* 6:14–34.
- Korotev R. L. 2005. Lunar geochemistry as told by lunar meteorites. *Chemie Der Erde-Geochemistry* 65:297–346.
- Korotev R. L., Jolliff B. L., Zeigler R. A., and Haskin L. A. 2003. Compositional constraints on the launch pairing of three brecciated lunar meteorites of basaltic composition. *Antarctic Meteorite Research* 16:152–175.
- Korotev R. L. and Zeigler R. A. 2007. Keeping up with the lunar meteorites (abstract #1340). 38th Lunar and Planetary Science Conference. CD-ROM.
- Lindsley D. H. 1983. Pyroxene thermometry. *American Mineralogist* 68: 477–493.
- Lindsley D. H., Papike J. J., and Bence A. E. 1972. Pyroxferroite: breakdown at low pressure and high temperature. *Lunar Science* 3:483–485.
- Liu Y., Hill E., Patchen A., and Taylor L. A. 2007. New lunar meteorite MIL 05035: Petrography and mineralogy (abstract #2103). 38th Lunar and Planetary Science Conference. CD-ROM.
- Longhi J. 1991. Comparative liquidus equilibria of hypersthene-non-native basalts at low pressure. *American Mineralogist* 76:785–800.
- Longhi J. 2002. Some phase equilibrium systematics of lherzolite melting. *Geochemistry Geophysics Geosystems* 3, doi:10.1029/2001GC000204.
- Lu F., Taylor L. A., and Jin Y. 1989. Basalts and gabbros from Mare Crisium: Evidence for extreme fractional crystallization. Proceedings, 19th Lunar and Planetary Science Conference. pp. 199–207.
- McKay G., Wagstaff J., and Le L. 1991. REE distribution coefficients for pigeonite: Constraints on the origin of the mare basalt europium anomaly, III. LPI Technical Report 91-03:27–28.
- McKay G., Wagstaff J., and Yang S. R. 1986. Clinopyroxene REE distribution coefficients for shergottites—The REE content of the Shergotty melt. *Geochimica et Cosmochimica Acta* 50:927–937.
- Mikouchi T. 1999. Shocked plagioclase in the lunar meteorites Yamato-793169 and Asuka-881757: Implications for their shock and thermal histories. *Antarctic Meteorite Research* 12:151–167.
- Misawa K., Tatsumoto M., Dalrymple G. B., and Yanai K. 1993. An extremely low U/Pb source in the Moon—U-Th-Pb, Sm-Nd, Rb-Sr, and <sup>40</sup>Ar-<sup>39</sup>Ar isotopic systematics and age of lunar meteorite Asuka-881757. *Geochimica et Cosmochimica Acta* 57:4687–4702.
- Neal C. R., Hacker M. D., Snyder G. A., Taylor L. A., Liu Y. G., and Schmitt R. A. 1994. Basalt generation at the Apollo 12 site, part 1: New data, classification, and re-evaluation. *Meteoritics* 29: 334–348.
- Neal C. R. and Taylor L. A. 1992. Petrogenesis of mare basalts: A record of lunar volcanism. *Geochimica et Cosmochimica Acta* 56:2177–2211.
- Nishiizumi K., Hillebrand D. J., and Welten K. C. 2006. Exposure and terrestrial histories of lunar meteorites LAP 02205/02224/02226/02436, MET 01210, and PCA 02007 (abstract #2369). 37th Lunar and Planetary Science Conference. CD-ROM.
- Norman M. D., Duncan R. A., and Huard J. J. 2006. Identifying impact events within the lunar cataclysm from <sup>40</sup>Ar-<sup>39</sup>Ar ages and compositions of Apollo 16 impact melt rocks. *Geochimica et Cosmochimica Acta* 70:6032–6049.
- Nyquist L. E. and Shih C.-Y. 1992. The isotopic record of lunar volcanism. *Geochimica et Cosmochimica Acta* 56:2213–2234.
- Nyquist L. E., Shih C.-Y., and Reese Y. D. 2007. Sm-Nd and Rb-Sr ages for MIL 05035: Implications for surface and mantle sources (abstract #1702). 38th Lunar and Planetary Science Conference. CD-ROM.

- Oba T. and Kobayashi Y. 2001. The mineral assemblage of symplectites in lunar meteorite Asuka-881757. *Antarctic Meteorite Research* 14:21–27.
- Ostertag R. 1983. Shock experiments on feldspar crystals. Proceedings, 14th Lunar and Planetary Science Conference. pp. 364–376.
- Papike J. J., Karner J. M., and Shearer C. K. 2003. Determination of planetary basalt parentage: A simple technique using the electron microprobe. *American Mineralogist* 88:469–472.
- Papike J. J., Ryder G., and Shearer C. K. 1998. Lunar samples. In *Planetary materials*. Reviews in Mineralogy, vol. 36. pp. E1–E234.
- Phinney W. C. and Morrison D. A. 1990. Partition coefficients for calcic plagioclase: Implications for Archean anorthosites. *Geochimica et Cosmochimica Acta* 54:1639–1654.
- Rhodes J. M. and Hubbard N. J. 1973. Chemistry, classification and petrogenesis of Apollo 15 mare basalts. Proceedings, 4th Lunar Science Conference, vol. 2. pp. 1127–1148.
- Ryder G. and Schuraytz B. C. 2001. Chemical variation of the large Apollo 15 olivine-normative mare basalt rock samples. *Journal of Geophysical Research* 106:1435–1451.
- Schaal R. B., Horz F., Thompson T. D., and Bauer J. F. 1979. Shock metamorphism of granulated lunar basalts. Proceedings, 10th Lunar and Planetary Science Conference. pp. 2547–2571.
- Schnare D. W., Day J. M. D., Norman M. D., Liu Y., and Taylor L. A. 2008. A laser-ablation ICP-MS study of Apollo 15 low-titanium olivine-normative and quartz-normative mare basalts. *Geochimica et Cosmochimica Acta* 72:2556–2572.
- Slater V. P., Thompson C. K., Nettles J., Milam K., Stockstill K. R., Cahill J., Anand M., and Taylor L. A. An evaluation of the igneous crystallization programs—MELTS, MAGPOX, and COMAGMAT part II: Importance of magmatic  $fO_2$ . 34th Lunar and Planetary Science Conference. CD-ROM.
- Snyder G. A., Taylor L. A., and Neal C. R. 1992. A chemical model for generating the sources of mare basalts: Combined equilibrium and fractional crystallization of the lunar magmasphere. *Geochimica et Cosmochimica Acta* 56:3809–3823.
- Stöffler D., Keil K., and Scott E. R. D. 1991. Shock metamorphism of ordinary chondrites. *Geochimica et Cosmochimica Acta* 55:3845–3867.
- Takeda H., Arai T., and Saiki K. 1993. Mineralogical studies of lunar meteorite Yamato-793169, a mare basalt. *Proceedings of the NIPR Symposium on Antarctic Meteorites* 6:3–13.
- Taylor L. A., Kullerud G., and Bryan W. B. 1971. Opaque mineralogy and textural features of Apollo 12 samples and a comparison with Apollo 11 rocks. Proceedings, 2nd Lunar Science Conference, vol. 1. pp. 855–871.
- Taylor L. A., Uhlmann D. R., Hopper R. W., and Misra K. C. 1975. Absolute cooling rates of lunar rocks—Theory and application. Proceedings, 6th Lunar Science Conference. pp. 181–191.
- Taylor L. A., Onorato P. I. K., and Uhlmann D. R. 1977. Cooling rate estimations based on kinetic modelling of Fe-Mg diffusion in olivine. Proceedings, 8th Lunar Conference. pp. 1581–1592.
- Terada K., Sasaki Y., Anand M., Joy K. H., and Sano Y. 2007. Uranium-lead systematics of phosphates in lunar basaltic regolith breccia, Meteorite Hills 01210. *Earth and Planetary Science Letters* 259:77–84.
- Thaisen K. G. and Taylor L. A. Forthcoming. Meteorite fusion crust variability. *Meteoritics & Planetary Science*.
- Thalmann C., Eugster O., Herzog G. F., Klein J., Krahenbuhl U., Vogt S., and Xue S. 1996. History of lunar meteorites Queen Alexandra Range 93069, Asuka-881757, and Yamato-793169 based on noble gas isotopic abundances, radionuclide concentrations, and chemical compositions. *Meteoritics & Planetary Science* 31:857–868.
- Thompson C. K., Slater V. P., Stockstill K. R., Anand M., Nettles J., Milam K., Cahill J., and Taylor L. A. An evaluation of the igneous crystallization programs—MELTS, MAGPOX, and COMAGMAT part I: Does one size fit all? (abstract). 34th Lunar and Planetary Science Conference. CD-ROM.
- Warren P. H. 1985. The magma ocean concept and lunar evolution. *Reviews in Earth and Planetary Sciences* 13:201–240.
- Warren P. H. and Kallemeyn G. W. 1993. Geochemical investigation of two lunar mare meteorites: Yamato-793169 and Asuka-881757. *Proceedings of the NIPR Symposium on Antarctic Meteorites* 6:35–57.
- Yanai K. 1991. Gabbroic meteorite Asuka-31: Preliminary examination of a new type of lunar meteorite in the Japanese collection of Antarctic meteorites. Proceedings, 21st Lunar Planetary Science Conference. pp. 317–324.
- Yanai K. and Kojima H. 1991. Varieties of lunar meteorites recovered from Antarctica. *Proceedings of the NIPR Symposium on Antarctic Meteorites* 4:70–90.
- Zeigler R. A., Korotev R. L., and Jolliff B. L. 2007. Miller Range 05035 and Meteorite Hills 01210: Two basaltic lunar meteorites, both likely source crater-paired with Asuka-881757 and Yamato-793169 (abstract #2110). 38th Lunar and Planetary Science Conference. CD-ROM.
- Zinner E. and Crozaz G. 1986a. A method for the quantitative measurement of rare earth elements by ion microprobe. *International Journal of Mass Spectrometry and Ion Processes* 69:17–38.
- Zinner E. and Crozaz G. 1986b. Ion probe determination of the abundances of all the rare earth elements in single mineral grains. In *Secondary ion mass spectrometry, SIMS V*, edited by Benninghoven A., Colton R. J., Simons D. S., and Werner H. W. New York: Springer-Verlag. pp. 444–446.